Università degli Studi di Milano-Bicocca

Facoltà di Medicina e Chirurgia

Corso di Dottorato in Tecnologie Biomediche (Ciclo XXII)

IMAGING OF LUNG METABOLIC ACTIVITY BY MEANS OF POSITRON EMISSION TOMOGRAPHY DURING ACUTE LUNG INJURY

Coordinatore: Prof.ssa Marina Del Puppo

Tutor: Prof.ssa Cristina MESSA

Tesi di dottorato di:

Dott. Giacomo BELLANI

Matricola 534077

Anno Accademico 2008-2009

Summary

Introduction

Acute Lung Injury (ALI) and Acute Respiratory Distress Syndrome (ARDS)

Acute Lung Injury (ALI) and Acute Respiratory Distress Syndrome (ARDS) are characterized by acute onset of hypoxemic respiratory failure, and can be due either to pulmonary and extrapulmonary causes, leading to a massive pulmonary edema with alveolar flooding and loss of compliance [1]. In a recent perspective cohort study, the incidence of ARDS has been estimated in almost 80 cases per 100.000 person/year, with a mortality rate around 40 % [2] and significant long-term disabilities [3]. Among the supportive therapies proposed so far, mechanical ventilation represents a cornerstone, in order to maintain an acceptable oxygenation and carbon dioxide removal, given the marked hypoxemia, and the loss of respiratory system compliance. Several experimental and clinical data indicate the role of polymorphonuclear leukocytes (PMNs) in initiating and perpetuating the syndrome [4]. PMNs are widely represented in the bronchoalveolar lavage fluids [5] and in the histological specimens from ARDS patients. Furthermore, several animal ALI model are dependent form PMNs [6] and, despite ARDS can develop in severely neutropenic patients [7], pulmonary function frequently deteriorates in patients with lung injury as neutropenia resolves [8].

Once ARDS has been triggered, mechanichal ventilation itself can represent a powerful noxious stimulus, usually referred as Ventilator Induced Lung Injury (VILI). Since the first pioneeristic reports by Dr. Kolobow and coworkers [9], the subject has received a deep interest. The scenario where this phenomena takes place is represented by a “wet” lung with alveolar instability and areas who collapse, leaving little room for ventilation. The alveoli of the remaining “baby lung” [10], which has to receive the entire minute ventilation, will be abnormally stretched and overdistended, particularly if the tidal volume is not properly reduced. Moreover, a given fraction of alveoli will be collapsed at end-exhalation, but will be progressively re-opened by the tidal ventilation, thus undergoing a cyclic recruitment/derecruitment [11, 12]. Finally, it has been shown by a mathematical model that at the border between collapsed and aerated parenchyma a shearing force 5-fold greater than the airway pressure can develop [13]. All the aforementioned forces can determine a local inflammatory response either by direct parenchymal disruption, or mediated by the activation of mechanoceptor systems [14], further enhancing the injury related to the “primitive” ARDS process; according to recent theories (biotrauma [15]) the release of cytochines from the lung in the blood stream might affect the function of different organs (particularly if already primed by other inflammatory stimuli [16]), increasing the risk of MOF and death [17]. The importance of this phenomena was strengthened by the finding of a decreased ARDS mortality decreased when the tidal volume was reduced from 12 to 6 ml/kg; the decreased mortality was also associated to a reduction of one proinflammatory chemokine, IL-6 [18]. Since the beneficial effect of an approach

promoting alveolar recruitment and avoiding cycling opening and closure of the alveoli has been repeatedly suggested [11, 19, 20], a number of multicenter trial comparing higher versus lower PEEP levels was recently conducted, failing however to show a benefit on mortality rate from the higher PEEP approach [21, 22]. Moreover it should not be forgotten that even if the ventilatory settings are optimized, ARDS-affected lungs will necessarily exploit regional expansion heterogeneity; in other words, the PEEP level necessary for adequately preventing expiratory collapse of certain regions is very likely to determine regional over-distension of other regions.

Most of the aforementioned processes of recruitment/derecruitment and overdistension can be adequately imaged by means of computed tomography (CT) [23]. CT allows to visualize and quantify the amount of recruitment induced by PEEP [24] or by a Recruitment Manoeuver, [25] providing at the same time information concerning the regional mechanisms of action of PEEP. The interaction between PEEP and tidal volume in determining the amount of tidal alveolar recruitment/derecruitment can be detected as well [26]. Polymorphonuclear leukocytes (PMNs) play a key role in the onset and perpetuation of the VILI [27-30]. In a very elegant study, Choudhury et al. demonstrated that mechanical ventilatory stress initiates pulmonary PMN sequestration early in the course of VILI, and this phenomenon is associated with stretch induced inflammatory events[31]. Zhang et al. incubated human PMNs with broncho-alveolar lavage fluids obtained in patients ventilated either with a conventional or a protective strategy, showing a neat increase of the PMNs' activity in the former case [32]. Pretreatment of animals with

Granulocyte Colony Stimulation factor worsened the effect of high-tidal volume ventilation in rats [33].

However, despite the growing bulk of evidence concerning VILI, most of the current knowledge on the subject derives from experimental data obtained in animals and indirect data obtained in ALI/ARDS patients; thus the actual relevance of the aforementioned mechanisms in the clinical setting remains somehow speculative.

Positron Emission Tomography

Positron Emission Tomography (PET) is a functional imaging technique which relies on the detection of photons generated by the annihilation of a positron emitted by an instable isotope labeling a compound administered to a subject.[34]

In the daily clinical practice PET is used, in the vast majority of cases, for cancer staging and follow-up. PET, however, is an extremely flexible technique, that allows the in-vivo imaging of several functions, dependently on which tracer is used; for this reason PET has been applied, mainly for research purposes, to a large number of different diseases both in the clinical and pre-clinical setting; in the field of intensive care medicine most of the focus has been put on acute lung injury (ALI) and acute respiratory distress syndrome (ARDS).

A PET scanner is basically constituted by a ring of detectors surrounding the patient. The imaging procedure requires the administration of a biologically active molecule substituted in one atom with an unstable isotope, which decays with the emission of a positron. The positron is the anti-particle of an electron; thus, as soon

as the positron encounters one electron of the surrounding matter the two particles annihilate, and the masses are transformed in two photons, travelling in two opposite directions on the same line. When two photons are detected simultaneously (or, more appropriately, within a delay of nanoseconds) by two detectors of the ring an "event" is registered along the line connecting the detectors.

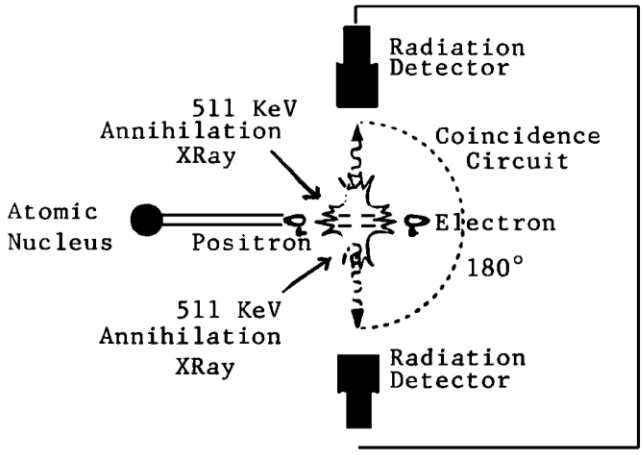

Principles of Decay and Detection

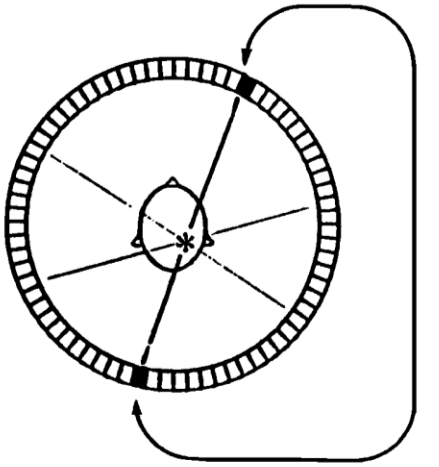

PET Detector Ring Coincidence Imaging

After having collected several millions of events it is possible, in analogy to a computed tomography (CT) acquisition, to reconstruct a planar image of the spatial distribution of the tracer, by using the "classical" Filtered Back-Projection, or, more recently, the ordered subset expectation maximization (OSEM) iterative algorithm. A modern PET scanner is constituted by a number of adjacent rings, so that a field of view 15-20 cm wide can be imaged at once.

However, the feature unique to PET does not reside much in the acquisition equipment, but in the tracers employed. Indeed the isotopes commonly used are 11-carbon, 13-nitrogen, 15-oxygen and 18-fluoride (which can be used as a substitute for hydrogen). It is thus possible to label virtually anyy molecule without altering its structure and, consequently, its biological properties; consequently PET can be used to image virtually any physiological process that can be individuated by following the spatial and temporal kinetic of one biological molecule. In the last decades hundreds of tracers have been developed and applied, mainly for research purposes.[35]

Table 1 reports some of the tracers that have been described and used for studying lung function.

Tracer	**Imaged Function**
[14C]CO	Regional blood volume
[18F]Fluorcaptopril	Pulmonary Angiotensin-converting Enzyme (ACE) expression, binding and inhibition
[13N]N2 (injected)	Regional perfusion and gas exchange (i.e. regional ventilation shunting blood flow, gas trapping)
[13N]N2 (inhaled)	Regional aeration and ventilation
[15O]H2O	Regional perfusion and extravascular lung water
68Ga-transferrin	Endothelial permeability
[^{11}C]PK11195	Presence of macrophages (specifically binds benzodiazepine peripheral receptors)

Studies employing [^{18}F]FDG

[^{18}F]fluoro-2-deoxy-D-glucose is an analog of glucose, which is uptaken by cells by the same transporters and at the same rate of glucose; the molecule undergoes to the first reaction of the respiratory chain, i.e. phosphorilation. However due to the absence of one oxygen atom the [^{18}F]FDG cannot proceed any further towards Krebs cycle and it is trapped in the cells. This is not the case only in hepatocytes, expressing the enzyme hexokynase which can de-phosphorilate [^{18}F]FDG making for it possible to leave the cells. In this way the accumulation of ^{18}FDG detected by PET is proportional to the intensity of glycolitic metabolism of the cells. Because of this property PET was originally devised for the study of brain metabolism, which heavily depends on glucose; however the burst of PET into clinical practice has been allowed by the fact that [^{18}F]FDG is actively uptaken by neoplastic cells from many different tumors, making PET an invaluable tool for staging and differential diagnosis of neoplasm.

In order to quantitate the uptake of 18FDG two kind of methods have been mainly used, so far[40]. The first class, “semi-quantitative”, routinely used in the clinical practice, relies on the use of the standardized uptake value (SUV), defined as the tissue concentration of tracer as measured by a PET scanner divided by the activity injected divided by body weight. Quantitative methods are based on the application of mathematical multi-compartmental models, fitted to the tracer time course. The Solokoff model assumes the presence of three compartments for [^{18}F]FDG (blood, tissutal precursor for phosphorilation and phopsphorilated), with

three time constants, expressing the rate of passage of FDG among the different compartments. Later, the simplified Patlak's graphical analysis was proposed: the ratio of tissue to plasma activity is plotted as a function of the ratio of the integral of plasma activity normalized to plasma activity. The experimental points are fitted with a linear regression whose slope represents the net uptake of FDG (Ki) and the intercept represents the initial volume of distribution. [Figura?] It is important to underline that both models have been devised for brain and subsequently used in the lungs, although their applicability in this organ might be debatable, due to the important anatomical differences. For this reason more sophisticated models have been specifically developed for the lung. [41]

Increased [^{18}F]FDG signal has been reported in the course of several experimental and clinical inflammatory processes in the lungs. The uptake of [^{18}F]FDG occurs primarily by activated neutrophils, whose metabolism (especially during the respiratory burst triggered by the rolling and adhesion phases) is heavily dependent on anaerobic glycolisis, requiring an elevated uptake of glucose. Microautoradiographic studies confirmed that, after in vivo administration of [^{18}F]FDG or ex-vivo incubation with 3HDG (deoxyglucose labeled with tritium) the only type of cells emitting radiation was neutrophils [42-44], even if other cell types such as macrophages were numerically more abundant[45]. In keeping with this finding it has been shown that, in a model of ventilator induced lung injury (VILI) the depletion of neutrophils, without affecting other cellular types, causes, basically, a disappearance of the [^{18}F]FDG signal.

PET with [^{18}F]FDG has been used to evaluate the inflammatory response in a number of experimental models of lung injury, including the administration of streptococcus pneumonia [42], oleic acid, endotoxin [46, 47] and bleomycin, Ventilator Induced Lung Injury (VILI) and smoke inhalation.

In an ovine model of VILI, in which one of the two lungs was injured by promoting alveolar overexpansion (by means of high peak pressure) and collapse (by means of a negative end-expiratory pressure) the injured lung shows a pronouncedly increase uptake of [^{18}F]FDG in comparison with the uninjured lung after only 90 minutes of injurious ventilation; at this time point, despite the injured lung had a marked loss of aeration aeration, gas exchange was only modestly deranged, probably because, as shown by the ventilation perfusion PET scan (see below) in most animals the perfusion had been redirected to the non-injured lung by the mechanism of pulmonary hypoxic vasoconstriction. [48]

PET with [^{18}F]FDG has been used in humans to image lung metabolic activity (likely to reflect inflammation) in the course of several types of lung disease, including asthma[49, 50], COPD[50], infection [51] and rejection of lung's transplant. In all such conditions PET allowed the imaging of lung's inflammation. Among eight patients at risk for the development of ALI, three of the four patients subsequently developing ALI had a "diffuse" uptake of FDG (i.e. involving both nonaerated or poorly aerated and normally aerated regions on CT), while in the patients subsequently not developing ALI the uptake of [^{18}F]FDG was confined to the regions of poor or absent aeration [52].

Finally, in healthy volunteers, after endobronchial instillation of 4 ng/kg of bacterial endotoxin, PET shows an increased [^{18}F]FDG uptake in the instilled bronchus; this is associated with an increased count of neutrophils in the bronchoalveolar lavage fluid. [53] This model, resembling under many aspects the inflammatory reaction characteristic of ALI (although confined to a small region of the lung), has been used to test the anti-inflammatory properties of some drugs. Indeed a significant reduction of [^{18}F]FDG uptake was obtained following the administration of lovastatin, but not of recombinant human activated protein C. [54] As suggested by the authors, this work provide evidence of the potential utility of PET with [^{18}F]FDG as a biomarker for neutrophilic inflammation and suggest that this tool may be useful during the early phases of drug development for testing the clinical efficacy of novel therapies.

Aims of the study

Acute Lung Injury (ALI) and Acute Respiratory Distress Syndrome (ARDS) are associated with a high mortality and significant long term morbidity [2, 55, 56]. While ALI/ARDS was originally considered to affect the lung diffusely, Computed Tomography (CT) scan studies indicated that areas of lung with normal aeration could be preserved, and coexist with poorly and non-aerated tissue, leading to the "baby-lung" concept [10].

It is accepted that inflammation and neutrophils (PMNs) play a key role in ALI/ARDS [4, 57, 58] and that their accumulation is a hallmark of ALI, despite the fact that ARDS can develop in severely neutropenic patients [7]. Moreover, PMNs

are primary effectors of Ventilator-Induced Lung Injury [33, 59, 60], which can aggravate ALI/ARDS.

Positron Emission Tomography (PET) with [^{18}F]fluoro-2-deoxy-D-glucose (^{18}FDG) [49, 61-64] can be used to image and quantitate cellular metabolic activity *in-vivo*. In several lung inflammatory processes, both in humans [51, 53] and in animal models [42, 43, 45, 48, 65], the increased metabolic activity can be ascribed, almost exclusively, to PMNs activation.

In patients with ALI/ARDS, it is unknown whether PMNs activation is diffuse throughout the entire lung, as it has been suggested for the increase in vascular permeability [66], or patchy, as is the increase in lung density [67]. Gaining knowledge on the distribution of PMNs activity and its relationship to lung density is important because it could offer insights into the pathophysiology of ALI/ARDS. For example, metabolic activation confined to poorly and non-aerated areas would indicate that the baby lung is spared by activated inflammatory cells, whereas activation confined to aerated areas would suggest that regional collapse may protect tissue from inflammatory cells activation, triggered instead by ventilatory stretch. Moreover, knowing the intensity and/or the regional distribution of the inflammatory process might lead to better tailoring of individual therapeutic and ventilatory strategies. However, the methods currently available to monitor the presence of PMNs in the lungs, like broncho-alveolar lavage [68] and lung biopsy [69], are unable to provide comprehensive informations on the topographical distribution of lung involvement.

Consequently, in the **first phase** of the study, we combined ^{18}FDG-PET and CT imaging to assess the magnitude and spatial distribution of PMNs activity, and test whether activation occurred only within a certain lung density range.

In the second phase of the study we focused on the inflammatory stimulus represented by Mechanical Ventilation (see above the section on VILI). One of the mechanisms that has been claimed as responsible for the genesis of VILI has been the cyclic recruitment and derecruitment of alveolar lung units, sometimes referred to as “atelectrauma”; neutrophils have been shown to play a key role in this type of injury. Most of the data on this mechanism derive from animal experiments, which can mimic the clinical condition only to a certain extent and to the date no direct evidence exists that atelectrauma plays, in fact a role in patients affected by ALI/ARDS. Moreover in a quite complex paper Chiumello et al. translated into clinical terms the concepts of stress and strain [70]. Stress is the force generated by lung parenchyma in response to an external load, clinically equivalent to transpulmunary pressure while strain is the change, relative to the initial status, of the lungs’ size, clinically equivalent to the ratio of Tidal Volume over Functional Residual Capacity.

The aim of the **second phase** of the research project was to assess if regions undergoing cyclic recruitment/derecruitment do show an increased metabolic activity likely to reflect inflammation in patients affected by ALI/ARDS.

Materials and Methods

Investigational protocol

The protocol was approved by our institution's ethical committee; informed consent was obtained according to the committee's recommendations. Patients were recruited from the general Intensive Care Unit (ICU) of a university hospital.

Inclusion criteria were:

- diagnosis of ALI/ARDS according to the 1994 European/American Consensus conference [71], requiring mechanical ventilation
- planning by the attending physician of a thorax CT scan as part of the patient's clinical management.

Exclusion criteria were:

- pregnancy
- age < 18 years
- impossibility of patient's transport according to the attending physician
- lung surgery in the last four weeks
- oliguria (urinary output<0.5 ml/kg/hour) or anuria
- known or suspected cancer
- history of chronic lung disease

- logistical reasons (e.g. PET/CT camera unavailable until patient had lost eligibility criteria).

Once a patient was judged eligible for the study, the PET/CT scan was scheduled, usually within one or two days; on the day of the study, eligibility was confirmed. A total of fifteen patients were enrolled. The PET/CT study being usually performed around 2pm, the enteral or parenteral nutrition and any glucose-containing infusion were stopped at 6 a.m. to ensure a fasting period of at least 6-8 hours. In patients undergoing insulin therapy, this was stopped as well. Before transport from the ICU to the PET/CT facility, blood glucose was tested to confirm a level between 80 and 140 mg/dl.

Before transport, the following variables were measured with the patient on volume controlled ventilation at settings selected by the attending physician: hemodynamic variables (heart rate, invasive arterial blood pressure, central venous pressure and, if a pulmonary artery catheter was in place, pulmonary arterial pressure, pulmonary artery occlusion pressure, cardiac output by thermodilution); ventilatory settings (Positive End-Expiratory Pressure (PEEP), Respiratory Rate, Tidal Volume (V_T), Mean Airway Pressure, Inspired Oxygen Fraction (FiO_2)). Expiratory and inspiratory pauses were performed to measure, respectively, total PEEP ($PEEP_{tot}$, which includes intrinsic PEEP) and plateau pressure (P_{plat}). Respiratory system compliance (C_{rs}) was computed as: $C_{rs}=V_T/(P_{plat}-PEEP_{tot})$.

Blood gases were measured from arterial and, if available, mixed venous samples (AVL Omni 6, Roche). Venous admixture was computed according to the Berggren equation [72].

During transport, and throughout the permanence in the PET/CT facility, clinical care was provided by a physician and a nurse uninvolved in the study procedures. Mechanical ventilation was provided by an ICU ventilator, and invasive arterial blood pressure, ECG, peripheral oxygen saturation and expired CO_2 were continuously monitored. Ventilatory settings, sedation, and fluid therapy were maintained constant throughout the study period, unless clinically advised.

At the end of the study, collection of the aforementioned variables was repeated in the ICU.

Finally, we recorded the 28 days and ICU outcome (survival or death) of each patient.

Image acquisition

We used a GE Discovery ST (GE Medical Systems, Milwaukee, WI) PET/CT tomograph, with an axial field of view of approximately 18 cm (47 3.27-mm thick sections, separated by 0.48 mm intervals), equipped with an 8-slice CT. The section of thorax to be imaged was selected on the scout view just above the diaphragm. Once the selection was made, care was taken to avoid any further movement of the patient on the examination table. A spiral CT scan (140 KV, 80 mA, slice thickness 3.75 mm, no interval between slices) of the chosen section was obtained while holding the patient apneic (by switching the ventilator to Constant Positive Airway Pressure modality) at the same mean airway pressure as during mechanical ventilation, to ensure the best possible cross-registration between the CT scan and the PET acquisition to follow, performed during tidal ventilation. The patient was

then advanced to the PET detector; the tomograph ensures the cross-registration of the same axial field-of-view between the CT and the PET acquisition. A bolus of ^{18}FDG (approximately 300 MBq) was rapidly injected intravenously, five seconds after that the acquisition of sequential PET frames was started with the following protocol: 12 frames lasting 10 seconds each (12 × 10''), 10 × 30'', 8 × 300'', 1 × 600'', for a total imaging time of 57 minutes.

At the end of the PET scanning we acquired two additional sets of CT scans holding the airway pressure constant at the level of end-expiration (PEEP, CT_{EXP}) and end-inspiration (Plateau pressure, CT_{INSP}), to obtain images of the regional lung expansion induced by tidal ventilation.

Image analysis

Dynamic PET data were reconstructed by ordered-subset expectation maximization (OSEM) iterative algorithm [73-75] and corrected for decay, scatter, random counts, attenuation (using CT).

Images were analyzed with a software specifically developed in Matlab environment (Matlab R2007a, The Mathworks, Natick, MA). Lung fields (Region-Of-Interest, ROI_L) were manually outlined on the CT images, carefully avoiding the large airways, vessels and pleural effusions. The $ROI_{L,}$ displayed as thick yellow lines, were overlapped to the last frame of the corresponding PET scan, and the fused PET/CT image was used for a visual assessment of the location of ^{18}FDG uptake.

For quantitative image analysis, we used Patlak's graphical method [76]. Briefly, an additional ROI was defined in the center of the descending aorta over at least 15-20 slices [77], in order to determine the time course of blood activity. The activity in ROI_L divided by blood activity was plotted as a function of the integral of blood activity divided by blood activity (Figure 1). After a steady state in cellular ^{18}FDG uptake is reached, the plot follows straight line, whose slope indicates the ^{18}FDG uptake rate constant (Ki). As this parameter is expected to increase with the number of cells per voxel (e.g. in the case of increased CT density due to an increase in the ratio of pulmonary parenchyma-to-gas volume), we also normalized Ki by the mean fractional density of the lung, computed as $(CT_{MEAN}+1000)/1000$, where CT_{MEAN} is the average CT number of the ROI_L: $Ki_{DENS} = Ki/[(CT_{MEAN}+1000)/1000]$.

The original CT matrix, with a size of 512-by-512 pixels, was re-scaled to achieve the same dimension (128-by-128) and pixel size (4.5 mm) of the original PET image. This scaling process lowers the spatial resolution of CT to a level similar to that of PET.

Density based ROIs: In order to describe the intra-patient relationship between lung density and ^{18}FDG uptake, the original ROI_L was sub-segmented (relying on the down-scaled CT image) by allocating all the voxels within "bins" 100 Hounsfield Units (HU) wide (the first "submask" enclosed all the voxels between -1000 HU and -900 HU, the second one comprised all the voxels between -900 HU and -800 HU, and so forth). For each of these density-defined ROIs their Ki value (Ki_D) and mean CT value (CT_D) were computed. It has to be emphasized that Ki_D, as opposed to

Ki_{DENS}, is not a density-normalized Ki, rather it is a measure of the ^{18}FDG uptake rate of lung areas with a given density.

"Tissue compartments": We defined normally aerated ROIs (comprising voxels with CT attenuation between -900 and -501 HU) and "collapsed or consolidated" (i.e. non-aerated) ROIs (comprising voxels with CT attenuation between -100 and +100 HU), and we computed their Ki (Ki_{NA} and Ki_{CO}, respectively).

Intra-tidal recruitment derecruitment: The tissue with absent aeration on CT_{INSP} and CT_{EXP} was defined as tissue derecruited (D-D) throughout the respiratory cycle. The tissue with absent aeration on CT_{EXP} but whit normal or poor aeration on CT_{INSP} was defined as tissue undergoing cyclic recruitment derecruitment (R-D). For this ROIS we computed the Ki (Ki_{D-D} and Ki_{R-D}) respectively.

None of the aforementioned calculation was performed on a voxel-by-voxel basis, rather, on the activity arising from a given ROI, which is the average activity of the voxels in the ROI.

We also computed the relative weight of the normally aerated and "non-aerated" (-100 HU < CT < 100 HU) tissue, by summing the weight of the corresponding voxels and dividing it by the weight of the entire ROI_L. The weight of each voxel was computed as $[(CT_{vox}+1000)/1000]*Vol_{vox}$, where CT_{vox} and Vol_{vox} are the CT number and the volume of the voxel, respectively.

For each tissue compartment Computed Tomography-assessed Tidal Volume strain was defined as Vt_{CT} gas volume on CTINSP minus gas volume on CTEXP. Computed Tomography-assessed end expiratory lung volume ($EELV_{CT}$) was defined as gas volume on CT_{EXP}. Finally for each ROI strain was computed $Vt_{CT}/EELV_{CT}$.

Control data

In order to obtain control values, we performed a CT scan followed by a dynamic PET acquisition with the previously indicated parameters:

a) in four spontaneously breathing subjects, undergoing PET/CT for clinical indications, without a known pulmonary disease;

b) in two ICU patients, being mechanically ventilated (for 4 and 19 days) for a neurologic disorder, who had normal gas exchange (PaO_2/FiO_2 > 300 mmHg).

Statistics

SPSS 14.0 was used for statistical analysis (SPSS 14.0 , SPSS Inc., Chicago, IL). Although variables were normally distributed (as assessed by Kolgomorov-Smirnov Z test), given the relatively small sample size and the difference in size between groups, we chose to use the non-parametric Mann-Whitney U test for comparison between groups. Wilcoxon Signed-rank test was used for paired comparisons (baseline vs after PET/CT). Linear regression was used to assess correlation between variables. $P < 0.05$ was considered statistically significant.

Results

Analysis for the entire lung

The main demographic and clinical characteristics of the patients are shown in Table 1. None of the parameters differed between before and after the PET/CT study (*data not shown*).

In ALI/ARDS patients, the metabolic activity of the lungs was markedly elevated in comparison with controls, as shown by the Ki values (and Figure 2). This difference was still present after normalizing the Ki values for the lung density (Ki_{DENS}).

The inter-subject variability of these parameters was large (coefficients of variation were 67.8 % and 59.8%, respectively, see Table 2) and no difference was found in either Ki or Ki_{DENS} between ARDS of pulmonary and extrapulmonary origin. The metabolic activity of the whole lung did not correlate with whole-lung density (CT_{mean}) or with the relative weight of either collapsed or normally aerated tissue . However, patients with a greater level of metabolic activity of the lungs had a more severe derangement of gas exchange; indeed Ki values correlated negatively with PaO_2/FiO_2 (Figure 3A; r^2 =0.48, $p<0.05$) and positively with $PaCO_2$ (Figure 3B; r^2=0.64 ; $p<0.01$). While attempting to assess the relationship existing between the metabolic activity of the lungs and the potential injury arising from mechanical

ventilation we could not find significant correlations between either Ki or Ki_{DENS} and P_{plat} or duration of mechanical ventilation.

The metabolic activity of the normally aerated tissue (Ki_{NA}) of ALI/ARDS patients ($83.8 \pm 85.6 \bullet 10^{-4}$ ml/min/ml range 23.5-250) showed, on average a seven-fold increase when compared to controls ($12 \pm 33, \bullet 10^{-4}$ ml/min/ml), with a coefficient of variation much larger than the coefficient of variation than Ki_{CO} (102 vs 55% $p<0.05$).

Regional distribution of aeration abnormalities and 18F-FDG uptake.

When qualitatively describing the regional distribution of the ^{18}FDG uptake and its relationship with the regional density among the different patients, we recognized different patterns. While in six patients (55 %) the ^{18}FDG uptake was highest in the regions with highest density and progressively decreased in regions of lower density, in three patients (33 %) the areas of normal or poor aeration bore ^{18}FDG uptake similar to or greater than that of areas of higher density. Representative images of these two patterns are shown in figure 4. Finally, in two patients, the ^{18}FDG uptake was lower than in the other patients and homogenously distributed throughout the lungs.

Analogous results were found when plotting the Ki_D values as a function of their respective CT_D values (Figure 5). Three patients, showed a shape of the

relationship between CT_D and Ki_D very different from the rest of the population, i.e. characterized by the highest Ki_D values in the range of the normally or poorly aerated voxels. These patients were also those with the highest mean Ki and Ki_{DENS} values. These patients had a more severe derangement in gas exchange (PaO_2/FiO_2 123 ± 23 vs 180 ± 28 mmHg p=0.053 and $PaCO_2$: 59.9 ± 7.7 vs 41.0 ± 6.8 mmHg p<0.05) and in lungs' mechanical properties (P_{plat} 28.9 ± 1.9 vs 22.8 ± 5.8 cmH_2O p=0.087) than the rest of the patients.

Effect of mechanical ventilation

Atelectrauma

At end expiration the amount of non-aerated tissue was 33 ± 13 %; only a modest amount (8.8 ± 17 %) of this tissue underwent cyclic recruitment/derecruitment was small, corresponding to 2.9 ± 5.9 % of total lung weight. No systematic difference between KiD-R and KID-D was seen (figure 6A), even after normalization for density (Figure 6B). In 3 out of 11 patients undergoing this imaging protocol, the ratio KiD-R/KiD-D was greater than one; overall the ratio ratio KiD-R/KiD-D was correlated with plateau pressure (R^2=0.41, p<0.05, figure 7), but not with duration of mechanical ventilation or with the amount of tissue undergoing cyclic recruitment/derecruitment.

Role of stress and strain

At a global lung level no significant correlation was found between Ki_{WL} and the level of strain; however Ki_{NA} (but not Ki_{PA}) was correlated with strain (R2=0.36; $p<0.05$) of the respective tissue class (figure 8A and 8B).

An exponential relationship was found between Ki_{NA} and plateau pressure (Figure 9A): Ki values increase steeply for values of Pplat above 26-27 cmH2O. A linear correlation was also found between Pplat and Ki_{NA}/Ki_{WL} (Figure 9B). This ratio expresses the degree of metabolic activity of the normally aerated tissue in respect to the average activity of the lung, normalizing for between patients variability of KiWL. Analogous relationship were found when KiNA and KiNA% were plotted as a function of respiratory system compliance.

Discussion

This study shows that the lungs of patients with ALI/ARDS have an intense metabolic activity, likely to arise from neutrophils involved in the inflammatory process. The magnitude and distribution of this activity were very variable among our subjects. However, a consistent finding was that metabolic activation did not involve only the collapsed areas of the lung but also the areas detected by CT as being “normally aerated” (the “baby lung”). Moreover we showed that while in some patients the regional metabolic activity was greater in the areas of increased density, other patients showed the highest metabolic rate was present in areas of normal or poor aeration.

We enrolled a relatively small and heterogeneous cohort of patients: this is mainly due to the clinical and logistical difficulties of performing such a study; the same reasons did not allow performing the study at the same time point for all the subjects. However, while the number of patients can be seen as a limitation, we feel that the heterogeneous sample we enrolled is a representative sample of the ALI/ARDS patient population treated at our institution

We used PET/CT with ^{18}FDG to detect and quantify inflammation. This technique bears several advantages, namely the low invasiveness, the possibility of imaging a large fraction of the lungs at once and the cross registration with CT. ^{18}FDG, however, is a non-specific tracer, since it labels any cell with an intense

glucose uptake. Several studies, performed both in humans [51, 53] and in animal models [42, 43, 45, 48] have shown that, during pulmonary inflammatory processes, the ^{18}FDG signal can be attributed almost exclusively to activated PMNs. In a model of Ventilator-induced lung injury, not only the ^{18}FDG signal correlated with the number of PMNs detected in the lung parenchyma, but decreased substantially with progressive PMNs depletion.[48] In order to minimize the potential confounding effect of uptake from other cell types, we excluded all patients with diagnosis or suspicion of cancer. For these reasons it seems reasonable to assume that, in our patients, most of the ^{18}FDG signal arose from PMNs activated in the setting of inflammation.

In ALI/ARDS as well as in normal subjects the perfusion in the lung is not homogeneous [48, 78]; this is, however, unlikely to affect ^{18}FDG distribution, whose uptake has been repeatedly shown to be almost totally unrelated to regional perfusion, at least in other organs [79-83]. Indeed, in experimental models of unilateral lung injury induced by mechanical stretch [48] and smoke inhalation [64], the injured lung always showed greater ^{18}FDG uptake than the control one independent of whether the blood flow favoured or not the injured lung.

Ki values differed greatly among patients. Although this finding is in line with the well described heterogeneity of ALI/ARDS, it did not seem to be related to whether the cause of ALI/ARDS was pulmonary or extrapulmonary. The increase and inter-individual variability of Ki persisted when Ki was normalized by tissue density, to account for the effect that a greater amount of lung tissue per unit volume of lung might have on Ki. It is important to note that this normalization is

conservative [48], since it is expected to lead to an underestimation of metabolic rate when the increase in density is due to edema, as edema fluid does not contribute significantly to ^{18}FDG uptake [43].

In all ALI/ARDS patients metabolic activity was markedly increased in lung tissue with density between -900 and -500 HU, where in one patient the ^{18}FDG uptake was as high as 20-fold that of the average value measured in control patients. Previous studies showed that, despite preserved aeration, the “baby lung” bears functional abnormalities: while in the course of lobar pneumonia endothelial permeability increased only in the affected lobe, in ALI/ARDS patients lung permeability diffusely increased throughout the whole lung [84]. This study provides direct evidence that in ALI/ARDS the normally aerated parenchyma shows a substantially increased metabolic rate, likely to reflect the presence of activated inflammatory cells. This supports the concept that the ‘baby lung’ while appearing “normal” in terms of aeration, is indeed involved by the inflammatory process as much as the rest of the lung. Since the presence of neutrophilic activation can trigger and promote the evolution towards fibrosis during inflammatory lung disease [45], this mechanism might be responsible for the development of the fibrosis involving the non-dependent areas (usually normally aerated in the acute phase of the disease) demonstrated by the long-term CT follow up in ALI/ARDS survivors [85].

Another finding is that, when analyzing the regional distribution of Ki, and specifically its relationship with lung density, two patterns could be found: while in seven patients the greatest ^{18}FDG uptake rate could be seen in the regions with

greater density, this was not the case for other three, characterized by the highest metabolic activity in the range of the normally or poorly aerated voxels. In normal lungs Ki is expected to correlate with lung density, as was indeed the case for our control subjects: this is due to the fact that regions with an increased lung density have more tissue and less air. The absence of such a correlation, as noticed in three patients, can be explained in at least two ways, potentially co-existing. First the less-aerated tissue could have a metabolic activity actually lower than the more aerated one, but this difference would be offset or reduced by its greater density, which increases the number of metabolically active cells in each voxel. Second: as already discussed, the increase in lung density could be due to the presence of edema fluid, rather than alveolar collapse. In this case, two regions can have very different densities as measured by CT scan but similar cell mass per voxel unit: as edema fluid does not actively uptake ^{18}FDG the Ki values would be similar. The most likely hypothesis is that both scenarios co-exist, probably also within a patient. Interestingly, the three patients with the highest metabolic activity in the range of normally or poorly aerated densities had a higher plateau pressure (although it cannot be said whether the higher distending forces where the causes or the result of the abnormalities seen on PET), a more deranged gas exchange, and their clinical course was characterized by an absence of improvement in the LIS, one week after the PET/CT study, possibly also as a result of the injury perpetuated in the normally and poorly aerated regions by the inflammatory cells.

Conclusion

In conclusion, despite these preliminary results need to be confirmed and expanded in a larger sample of patients, this study shows that in patients with ALI/ARDS the metabolic activity of the lung is substantially increased across the entire lung density spectrum. This suggests that no region of the lung is spared by the presence of activated inflammatory cells; the intensity of this activation and its regional distribution, however, vary widely within and between subjects. Moreover we have been able to show an association between inflammation and stress and strain generated in the lung from mechanical ventilation.

References

1. Ware LB, Matthay MA, (2000) The acute respiratory distress syndrome. N Engl J Med 342: 1334-1349
2. Rubenfeld GD, Caldwell E, Peabody E, Weaver J, Martin DP, Neff M, Stern EJ, Hudson LD, (2005) Incidence and outcomes of acute lung injury. N Engl J Med 353: 1685-1693
3. Herridge MS, Cheung AM, Tansey CM, Matte-Martyn A, Diaz-Granados N, Al-Saidi F, Cooper AB, Guest CB, Mazer CD, Mehta S, Stewart TE, Barr A, Cook D, Slutsky AS, (2003) One-year outcomes in survivors of the acute respiratory distress syndrome. N Engl J Med 348: 683-693
4. Abraham E, (2003) Neutrophils and acute lung injury. Crit Care Med 31: S195-199
5. Pittet JF, Mackersie RC, Martin TR, Matthay MA, (1997) Biological markers of acute lung injury: prognostic and pathogenetic significance. Am J Respir Crit Care Med 155: 1187-1205
6. Prescott SM, McIntyre TM, Zimmerman G, (1999) Two of the usual suspects, platelet-activating factor and its receptor, implicated in acute lung injury. J Clin Invest 104: 1019-1020
7. Laufe MD, Simon RH, Flint A, Keller JB, (1986) Adult respiratory distress syndrome in neutropenic patients. Am J Med 80: 1022-1026
8. Azoulay E, Darmon M, Delclaux C, Fieux F, Bornstain C, Moreau D, Attalah H, Le Gall JR, Schlemmer B, (2002) Deterioration of previous acute lung injury during neutropenia recovery. Crit Care Med 30: 781-786
9. Kolobow T, Moretti MP, Fumagalli R, Mascheroni D, Prato P, Chen V, Joris M, (1987) Severe impairment in lung function induced by high peak airway pressure during mechanical ventilation. An experimental study. Am Rev Respir Dis 135: 312-315

10. Gattinoni L, Pesenti A, (2005) The concept of "baby lung". Intensive Care Med 31: 776-784
11. Carney DE, Bredenberg CE, Schiller HJ, Picone AL, McCann UG, Gatto LA, Bailey G, Fillinger M, Nieman GF, (1999) The Mechanism of Lung Volume Change during Mechanical Ventilation. Am J Respir Crit Care Med 160: 1697-1702
12. Muscedere JG, Mullen JB, Gan K, Slutsky AS, (1994) Tidal ventilation at low airway pressures can augment lung injury. Am J Respir Crit Care Med 149: 1327-1334
13. Mead J, Takishima T, Leith D, (1970) Stress distribution in lungs: a model of pulmonary elasticity. J Appl Physiol 28: 596-608
14. Vlahakis NE, Hubmayr RD, (2003) Response of alveolar cells to mechanical stress. Curr Opin Crit Care 9: 2-8
15. Uhlig S, Ranieri M, Slutsky AS, (2004) Biotrauma hypothesis of ventilator-induced lung injury. Am J Respir Crit Care Med 169: 314-315; author reply 315
16. Crimi E, Zhang H, Han RN, Del Sorbo L, Ranieri VM, Slutsky AS, (2006) Ischemia and Reperfusion Increases Susceptibility to Ventilator-induced Lung Injury in Rats. Am J Respir Crit Care Med
17. Ranieri VM, Suter PM, Tortorella C, De Tullio R, Dayer JM, Brienza A, Bruno F, Slutsky AS, (1999) Effect of mechanical ventilation on inflammatory mediators in patients with acute respiratory distress syndrome: a randomized controlled trial. Jama 282: 54-61
18. (2000) Ventilation with lower tidal volumes as compared with traditional tidal volumes for acute lung injury and the acute respiratory distress syndrome. The Acute Respiratory Distress Syndrome Network. N Engl J Med 342: 1301-1308
19. van Kaam AH, Lachmann RA, Herting E, De Jaegere A, van Iwaarden F, Noorduyn LA, Kok JH, Haitsma JJ, Lachmann B, (2004) Reducing atelectasis

attenuates bacterial growth and translocation in experimental pneumonia. Am J Respir Crit Care Med 169: 1046-1053

20. van Kaam AH, Haitsma JJ, De Jaegere A, van Aalderen WM, Kok JH, Lachmann B, (2004) Open lung ventilation improves gas exchange and attenuates secondary lung injury in a piglet model of meconium aspiration. Crit Care Med 32: 443-449

21. Brower RG, Lanken PN, MacIntyre N, Matthay MA, Morris A, Ancukiewicz M, Schoenfeld D, Thompson BT, (2004) Higher versus lower positive end-expiratory pressures in patients with the acute respiratory distress syndrome. N Engl J Med 351: 327-336

22. Meade MO, Cook DJ, Guyatt GH, Slutsky AS, Arabi YM, Cooper DJ, Davies AR, Hand LE, Zhou Q, Thabane L, Austin P, Lapinsky S, Baxter A, Russell J, Skrobik Y, Ronco JJ, Stewart TE, (2008) Ventilation strategy using low tidal volumes, recruitment maneuvers, and high positive end-expiratory pressure for acute lung injury and acute respiratory distress syndrome: a randomized controlled trial. Jama 299: 637-645

23. Gattinoni L, Caironi P, Pelosi P, Goodman LR, (2001) What has computed tomography taught us about the acute respiratory distress syndrome? Am J Respir Crit Care Med 164: 1701-1711

24. Gattinoni L, D'Andrea L, Pelosi P, Vitale G, Pesenti A, Fumagalli R, (1993) Regional effects and mechanism of positive end-expiratory pressure in early adult respiratory distress syndrome. Jama 269: 2122-2127

25. Henzler D, Pelosi P, Dembinski R, Ullmann A, Mahnken AH, Rossaint R, Kuhlen R, (2005) Respiratory compliance but not gas exchange correlates with changes in lung aeration after a recruitment maneuver: an experimental study in pigs with saline lavage lung injury. Crit Care 9: R471-482

26. Terragni PP, Rosboch G, Tealdi A, Corno E, Menaldo E, Davini O, Gandini G, Herrmann P, Mascia L, Quintel M, Slutsky AS, Gattinoni L, Ranieri VM, (2007)

Tidal hyperinflation during low tidal volume ventilation in acute respiratory distress syndrome. Am J Respir Crit Care Med 175: 160-166

27. Tsuno K, Miura K, Takeya M, Kolobow T, Morioka T, (1991) Histopathologic pulmonary changes from mechanical ventilation at high peak airway pressures. Am Rev Respir Dis 143: 1115-1120

28. Caironi P, Ichinose F, Liu R, Jones RC, Bloch KD, Zapol WM, (2005) 5-Lipoxygenase Deficiency Prevents Respiratory Failure during Ventilator-induced Lung Injury. Am J Respir Crit Care Med 172: 334-343

29. Imanaka H, Shimaoka M, Matsuura N, Nishimura M, Ohta N, Kiyono H, (2001) Ventilator-induced lung injury is associated with neutrophil infiltration, macrophage activation, and TGF-beta 1 mRNA upregulation in rat lungs. Anesth Analg 92: 428-436

30. Quinn DA, Moufarrej RK, Volokhov A, Hales CA, (2002) Interactions of lung stretch, hyperoxia, and MIP-2 production in ventilator-induced lung injury. J Appl Physiol 93: 517-525

31. Choudhury S, Wilson MR, Goddard ME, O'Dea KP, Takata M, (2004) Mechanisms of early pulmonary neutrophil sequestration in ventilator-induced lung injury in mice. Am J Physiol Lung Cell Mol Physiol 287: L902-910

32. Zhang H, Downey GP, Suter PM, Slutsky AS, Ranieri VM, (2002) Conventional mechanical ventilation is associated with bronchoalveolar lavage-induced activation of polymorphonuclear leukocytes: a possible mechanism to explain the systemic consequences of ventilator-induced lung injury in patients with ARDS. Anesthesiology 97: 1426-1433

33. Karzai W, Cui X, Heinicke N, Niemann C, Gerstenberger EP, Correa R, Banks S, Mehlhorn B, Bloos F, Reinhart K, Eichacker PQ, (2005) Neutrophil stimulation with granulocyte colony-stimulating factor worsens ventilator-induced lung injury and mortality in rats. Anesthesiology 103: 996-1005

34. Schuster DP, (1989) Positron emission tomography: theory and its application to the study of lung disease. Am Rev Respir Dis 139: 818-840

35. Harris RS, Schuster DP, (2007) Visualizing lung function with positron emission tomography. J Appl Physiol 102: 448-458
36. Schuster DP, Anderson C, Kozlowski J, Lange N, (2002) Regional pulmonary perfusion in patients with acute pulmonary edema. J Nucl Med 43: 863-870
37. Schuster DP, Howard DK, (1994) The effect of positive end-expiratory pressure on regional pulmonary perfusion during acute lung injury. J Crit Care 9: 100-110
38. Mintun MA, Dennis DR, Welch MJ, Mathias CJ, Schuster DP, (1987) Measurements of pulmonary vascular permeability with PET and gallium-68 transferrin. J Nucl Med 28: 1704-1716
39. Jones HA, Valind SO, Clark IC, Bolden GE, Krausz T, Schofield JB, Boobis AR, Haslett C, (2002) Kinetics of lung macrophages monitored in vivo following particulate challenge in rabbits. Toxicol Appl Pharmacol 183: 46-54
40. Chen DL, Mintun MA, Schuster DP, (2004) Comparison of methods to quantitate 18F-FDG uptake with PET during experimental acute lung injury. J Nucl Med 45: 1583-1590
41. Schroeder T, Vidal Melo MF, Musch G, Harris RS, Venegas JG, Winkler T, (2008) Modeling Pulmonary Kinetics of 2-Deoxy-2-[(18)F]fluoro-d-glucose During Acute Lung Injury. Acad Radiol 15: 763-775
42. Jones HA, Clark RJ, Rhodes CG, Schofield JB, Krausz T, Haslett C, (1994) In vivo measurement of neutrophil activity in experimental lung inflammation. Am J Respir Crit Care Med 149: 1635-1639
43. Chen DL, Schuster DP, (2004) Positron emission tomography with [18F]fluorodeoxyglucose to evaluate neutrophil kinetics during acute lung injury. Am J Physiol Lung Cell Mol Physiol 286: L834-840
44. Jones HA, Cadwallader KA, White JF, Uddin M, Peters AM, Chilvers ER, (2002) Dissociation between respiratory burst activity and deoxyglucose uptake in human neutrophil granulocytes: implications for interpretation of (18)F-FDG PET images. J Nucl Med 43: 652-657

45. Jones HA, Schofield JB, Krausz T, Boobis AR, Haslett C, (1998) Pulmonary fibrosis correlates with duration of tissue neutrophil activation. Am J Respir Crit Care Med 158: 620-628

46. Zhou Z, Kozlowski J, Schuster DP, (2005) Physiologic, biochemical, and imaging characterization of acute lung injury in mice. Am J Respir Crit Care Med 172: 344-351

47. Schuster DP, Brody SL, Zhou Z, Bernstein M, Arch R, Link D, Mueckler M, (2007) Regulation of lipopolysaccharide-induced increases in neutrophil glucose uptake. Am J Physiol Lung Cell Mol Physiol 292: L845-851

48. Musch G, Venegas JG, Bellani G, Winkler T, Schroeder T, Petersen B, Harris RS, Melo MF, (2007) Regional gas exchange and cellular metabolic activity in ventilator-induced lung injury. Anesthesiology 106: 723-735

49. Taylor IK, Hill AA, Hayes M, Rhodes CG, O'Shaughnessy KM, O'Connor BJ, Jones HA, Hughes JM, Jones T, Pride NB, Fuller RW, (1996) Imaging allergen-invoked airway inflammation in atopic asthma with [18F]-fluorodeoxyglucose and positron emission tomography. Lancet 347: 937-940

50. Jones HA, Marino PS, Shakur BH, Morrell NW, (2003) In vivo assessment of lung inflammatory cell activity in patients with COPD and asthma. Eur Respir J 21: 567-573

51. Jones HA, Sriskandan S, Peters AM, Pride NB, Krausz T, Boobis AR, Haslett C, (1997) Dissociation of neutrophil emigration and metabolic activity in lobar pneumonia and bronchiectasis. Eur Respir J 10: 795-803

52. Rodrigues RS, Miller PR, Bozza FA, Marchiori E, Zimmerman GA, Hoffman JM, Morton KA, (2008) FDG-PET in patients at risk for acute respiratory distress syndrome: a preliminary report. Intensive Care Med 34: 2273-2278

53. Chen DL, Rosenbluth DB, Mintun MA, Schuster DP, (2006) FDG-PET imaging of pulmonary inflammation in healthy volunteers after airway instillation of endotoxin. J Appl Physiol 100: 1602-1609

54. Chen DL, Bedient TJ, Kozlowski J, Rosenbluth DB, Isakow W, Ferkol TW, Thomas B, Mintun MA, Schuster DP, Walter MJ, (2009)

[18F]fluorodeoxyglucose positron emission tomography for lung antiinflammatory response evaluation. Am J Respir Crit Care Med 180: 533-539

55. Wheeler AP, Bernard GR, (2007) Acute lung injury and the acute respiratory distress syndrome: a clinical review. Lancet 369: 1553-1564

56. Yilmaz M, Iscimen R, Keegan MT, Vlahakis NE, Afessa B, Hubmayr RD, Gajic O, (2007) Six-month survival of patients with acute lung injury: prospective cohort study. Crit Care Med 35: 2303-2307

57. Lee WL, Downey GP, (2001) Neutrophil activation and acute lung injury. Curr Opin Crit Care 7: 1-7

58. Wittkowski H, Sturrock A, van Zoelen MA, Viemann D, van der Poll T, Hoidal JR, Roth J, Foell D, (2007) Neutrophil-derived S100A12 in acute lung injury and respiratory distress syndrome. Crit Care Med 35: 1369-1375

59. Sugiura M, McCulloch PR, Wren S, Dawson RH, Froese AB, (1994) Ventilator pattern influences neutrophil influx and activation in atelectasis-prone rabbit lung. J Appl Physiol 77: 1355-1365

60. Kawano T, Mori S, Cybulsky M, Burger R, Ballin A, Cutz E, Bryan AC, (1987) Effect of granulocyte depletion in a ventilated surfactant-depleted lung. J Appl Physiol 62: 27-33

61. Jones HA, (2005) Inflammation imaging. Proc Am Thorac Soc 2: 545-548, 513-544

62. Schuster DP, (1998) The evaluation of lung function with PET. Semin Nucl Med 28: 341-351

63. Musch G, Venegas JG, (2006) Positron emission tomography imaging of regional lung function. Minerva Anestesiol 72: 363-367

64. Schroeder T, Vidal Melo MF, Musch G, Harris RS, Winkler T, Venegas JG, (2007) PET Imaging of Regional 18F-FDG Uptake and Lung Function After Cigarette Smoke Inhalation. J Nucl Med 48: 413-419

65. Hartwig W, Carter EA, Jimenez RE, Jones R, Fischman AJ, Fernandez-Del Castillo C, Warshaw AL, (2002) Neutrophil metabolic activity but not

neutrophil sequestration reflects the development of pancreatitis-associated lung injury. Crit Care Med 30: 2075-2082

66. Sandiford P, Province MA, Schuster DP, (1995) Distribution of regional density and vascular permeability in the adult respiratory distress syndrome. Am J Respir Crit Care Med 151: 737-742

67. Maunder RJ, Shuman WP, McHugh JW, Marglin SI, Butler J, (1986) Preservation of normal lung regions in the adult respiratory distress syndrome. Analysis by computed tomography. Jama 255: 2463-2465

68. Perkins GD, Chatterjie S, McAuley DF, Gao F, Thickett DR, (2006) Role of nonbronchoscopic lavage for investigating alveolar inflammation and permeability in acute respiratory distress syndrome. Crit Care Med 34: 57-64

69. Papazian L, Doddoli C, Chetaille B, Gernez Y, Thirion X, Roch A, Donati Y, Bonnety M, Zandotti C, Thomas P, (2007) A contributive result of open-lung biopsy improves survival in acute respiratory distress syndrome patients. Crit Care Med 35: 755-762

70. Chiumello D, Carlesso E, Cadringher P, Caironi P, Valenza F, Polli F, Tallarini F, Cozzi P, Cressoni M, Colombo A, Marini JJ, Gattinoni L, (2008) Lung stress and strain during mechanical ventilation for acute respiratory distress syndrome. Am J Respir Crit Care Med 178: 346-355

71. Bernard GR, Artigas A, Brigham KL, Carlet J, Falke K, Hudson L, Lamy M, Legall JR, Morris A, Spragg R, (1994) The American-European Consensus Conference on ARDS. Definitions, mechanisms, relevant outcomes, and clinical trial coordination. Am J Respir Crit Care Med 149: 818-824

72. Warner MA, Divertie MB, Offord KP, Marsh HM, Helmholz HF, Jr., McMichan JC, (1983) Clinical implications of variation in total venoarterial shunt fraction calculated by different methods during severe acute respiratory failure. Mayo Clin Proc 58: 654-659

73. Schiepers C, Nyhuts J, Wu HM, Verma RC, (1997) PET with 18F-Fluoride: Effects of Iterative versus Filtered Backprojection Reconstruction on Kinetic Modeling. IEEE Trans Nucl Sci 44: 1591-1593

74. Lubberink M, Boellaard R, van der Weerdt AP, Visser FC, Lammertsma AA, (2004) Quantitative comparison of analytic and iterative reconstruction methods in 2- and 3-dimensional dynamic cardiac 18F-FDG PET. J Nucl Med 45: 2008-2015

75. Sondergaard HM, Madsen MM, Boisen K, Bottcher M, Schmitz O, Nielsen TT, Botker HE, Hansen SB, (2007) Evaluation of iterative reconstruction (OSEM) versus filtered back-projection for the assessment of myocardial glucose uptake and myocardial perfusion using dynamic PET. Eur J Nucl Med Mol Imaging 34: 320-329

76. Patlak CS, Blasberg RG, Fenstermacher JD, (1983) Graphical evaluation of blood-to-brain transfer constants from multiple-time uptake data. J Cereb Blood Flow Metab 3: 1-7

77. de Geus-Oei LF, Visser EP, Krabbe PF, van Hoorn BA, Koenders EB, Willemsen AT, Pruim J, Corstens FH, Oyen WJ, (2006) Comparison of image-derived and arterial input functions for estimating the rate of glucose metabolism in therapy-monitoring 18F-FDG PET studies. J Nucl Med 47: 945-949.

78. Musch G, Layfield JD, Harris RS, Melo MF, Winkler T, Callahan RJ, Fischman AJ, Venegas JG, (2002) Topographical distribution of pulmonary perfusion and ventilation, assessed by PET in supine and prone humans. J Appl Physiol 93: 1841-1851

79. Stewart EE, Chen X, Hadway J, Lee TY, (2006) Correlation between hepatic tumor blood flow and glucose utilization in a rabbit liver tumor model. Radiology 239: 740-750

80. Dunn RT, Willis MW, Benson BE, Repella JD, Kimbrell TA, Ketter TA, Speer AM, Osuch EA, Post RM, (2005) Preliminary findings of uncoupling of flow and metabolism in unipolar compared with bipolar affective illness and normal controls. Psychiatry Res 140: 181-198

81. Ronnemaa EM, Ronnemaa T, Utriainen T, Raitakari M, Laine H, Takala T, Pitkanen OP, Kirvela O, Knuuti J, Nuutila P, (1999) Decreased blood flow but

unaltered insulin sensitivity of glucose uptake in skeletal muscle of chronic smokers. Metabolism 48: 239-244

82. Nuutila P, Raitakari M, Laine H, Kirvela O, Takala T, Utriainen T, Makimattila S, Pitkanen OP, Ruotsalainen U, Iida H, Knuuti J, Yki-Jarvinen H, (1996) Role of blood flow in regulating insulin-stimulated glucose uptake in humans. Studies using bradykinin, [15O]water, and [18F]fluoro-deoxy-glucose and positron emission tomography. J Clin Invest 97: 1741-1747

83. Pitkanen OP, Laine H, Kemppainen J, Eronen E, Alanen A, Raitakari M, Kirvela O, Ruotsalainen U, Knuuti J, Koivisto VA, Nuutila P, (1999) Sodium nitroprusside increases human skeletal muscle blood flow, but does not change flow distribution or glucose uptake. J Physiol 521 Pt 3: 729-737

84. Kaplan JD, Calandrino FS, Schuster DP, (1991) A positron emission tomographic comparison of pulmonary vascular permeability during the adult respiratory distress syndrome and pneumonia. Am Rev Respir Dis 143: 150-154

85. Desai SR, Wells AU, Rubens MB, Evans TW, Hansell DM, (1999) Acute respiratory distress syndrome: CT abnormalities at long-term follow-up. Radiology 210: 29-35

Figure legends

Figure 1: Representative Patlak plot for one ARDS patient (corresponding, in the tables to patient #4, filled symbols) and for a spontaneously breathing control subject (empty symbols). ^{18}FDG activity in a region of interest (ROI), divided by blood activity, is plotted as a function of the time integral of blood activity divided by blood activity. The slope of the linear part of this relationship corresponds to the uptake rate of ^{18}FDG (Ki).

Figure 2: ^{18}FDG uptake rate (Ki) of the imaged lung **(Panel A)**, in the individual patients and as mean ± standard deviation. Despite large between-patients variability, Ki was higher than that of control subjects (dashed line denotes mean Ki of controls). This could not be ascribed solely to increased lung density, as the difference persisted after normalization by lung density **(Panel B).** * $P < 0.05$ patients versus controls

Figure 3: Correlation between lung's metabolic activity, expressed as uptake rate of ^{18}FDG (Ki), and PaO_2/FiO_2

Figure 4: Representative images of cross-registered CT and ^{18}FDG PET from two ALI/ARDS patients. The CT image was acquired during a respiratory pause at mean airway pressure. The gray scale is centered at -500 Hounsfield Units (HU) with a

width of 1250 HU. PET images represent the average pulmonary ^{18}FDG concentration over the last 20 minutes of acquisition (from 37 minutes to 57 minutes since ^{18}FDG administration); the color scale represents radioactivity concentration (kBq/cc). **Panel A:** ^{18}FDG distribution parallels that of the opacities detected on CT. **Panel B:** intense ^{18}FDG uptake can be observed in normally aerated regions (square 1), while activity is lower in the dorsal, "non-aerated" regions of both lungs (square 2).

Figure 5: Distribution of regional metabolic activity (Ki_D is the ^{18}FDG uptake rate of areas of specified density) as a function of regional lung density (CT_D), in the patients with ARDS/ALI (dotted lines) compared with that of the four controls (solid line: mean; bars: standard deviation). In some patients Ki_D increased linearly with CT_D (empty symbols); this was not the case for other patients (filled symbols). Note that, in all patients, the metabolic rate was systematically increased across the entire spectrum of normal lung attenuation.

Figure 7: The figure shows the positive correlation existing between ratio KiD-R/KiD-D and plateau pressure

Figure 8: Correlation between Ki_{NA} and Ki_{PA}) with strain of the respective tissue class.

Figure 9: An exponential relationship was found between Ki_{NA} and plateau pressure (Figure 9A): Ki values increase steeply for values of Pplat above 26-27 cmH2O. A linear correlation was also found between Pplat and Ki_{NA}/Ki_{WL} (Figure 9B).

Table 1:

Patient number	Mean ± s.d.
Age (years)	66 ± 13
Sex (M:F)	12:4
ARDS etiology (Pulm:ExP)	11:5
Outcome at ICU discharge (S:D)	11:5
Time on MV before study (days)	8.2 ± 7.3
Heart Rate (beats per min)	79 ± 13
MAP (mmHg)	83 ± 15
MPAP (mmHg)	29 ± 5
PaO_2/FiO_2 (mmHg)	163 ± 43
$PaCO_2$ (mmHg)	45 ± 8
FiO_2	0.58 ± 0.13
Venous Admixture	0.28 ± 0.04
$PEEP_{tot}$ (cmH_2O)	13 ± 2.7
Tidal Volume (ml/kg)	6.8 ± 1.1
Plateau pressure (cmH_2O)	24.8 ± 4.8
Respiratory Rate (breaths per min)	25.5 ± 5.2
Minute Ventilation (l/min)	10.6 ± 1.6
Blood Glucose (mg/dL)	125 ± 24

Patient's characteristics on the day of the study, collected before transport to the PET/CT facility. For dichotomic variables the last column reports the ratio between the two groups. List of abbreviations: F: Female, M: Male, S: Survived, D: Deceased, Pulm: Pulmonary, ExP: Extra-pulmonary, MV: Mechanical Ventilation, $PEEP_{tot}$: total Positive End-Expiratory Pressure (including intrinsic-PEEP), MAP: Mean Arterial Pressure: MPAP: Mean Pulmonary Arterial Pressure.

FIGURE 1

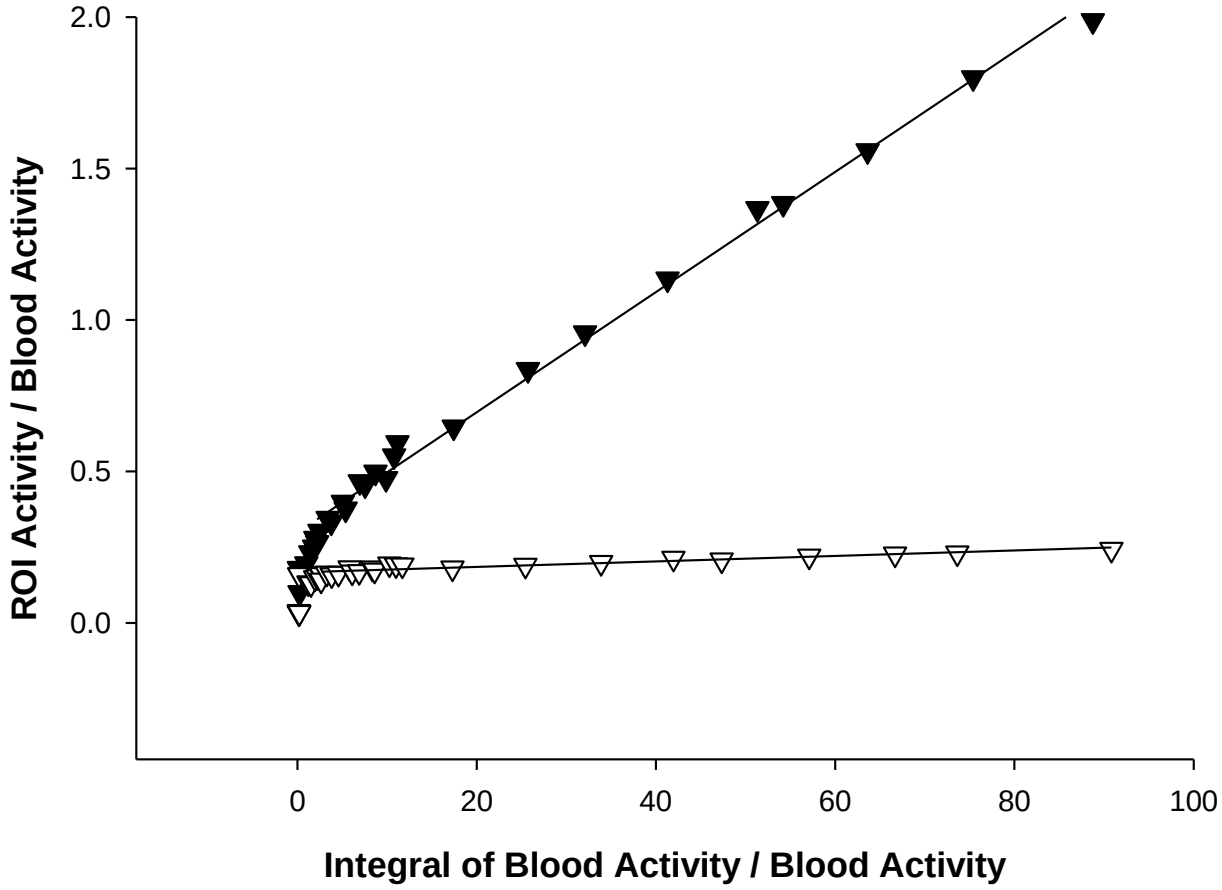
2.0
1.5
1.0
0.5
0.0
ROI Activity / Blood Activity
0
20
40
60
80
100
Integral of Blood Activity / Blood Activity

FIGURE 2A

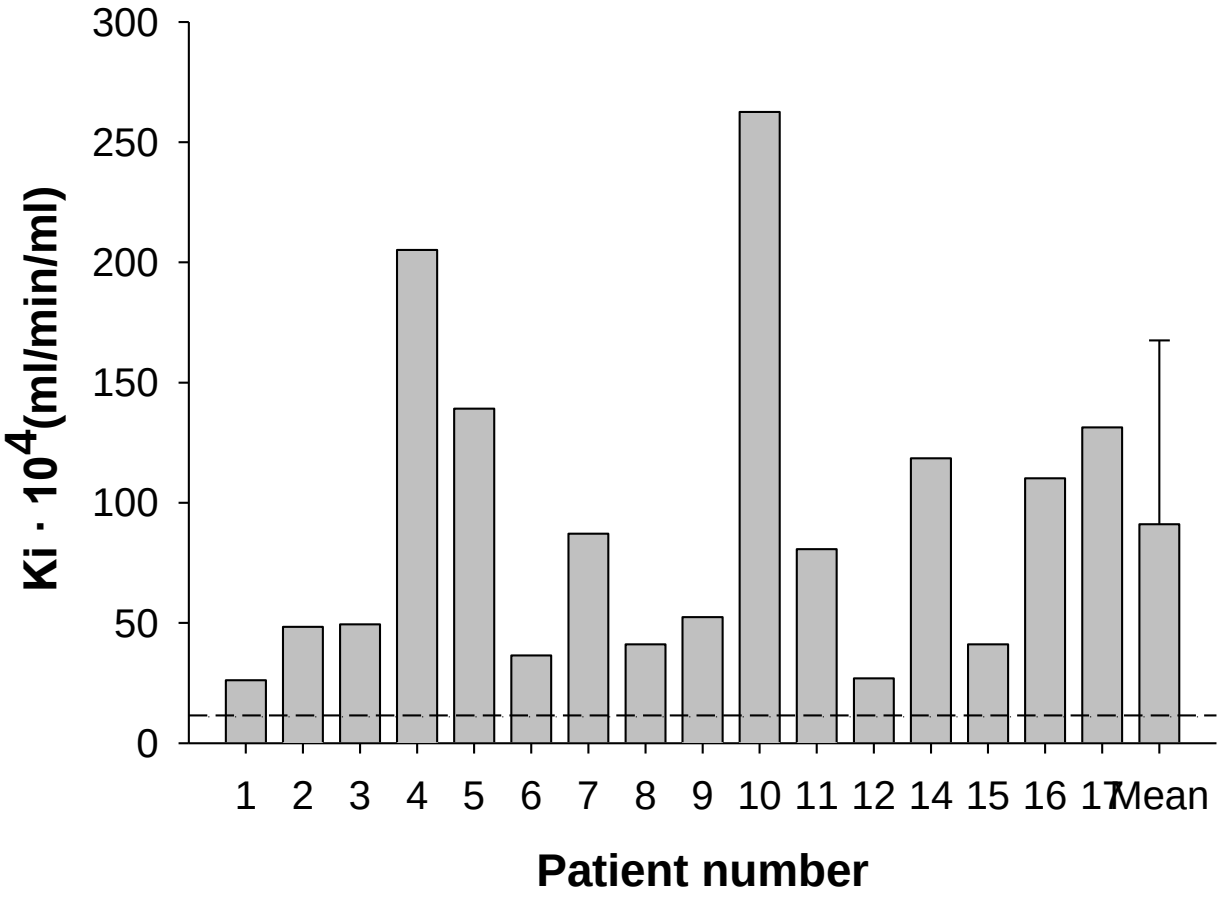
300
250
200
150
100
50
0
Ki · 10^4(ml/min/ml)
1
2
3
4
5
6
7
8
9
10
11
12
14
15
16
17
Mean
Patient number

FIGURE 2B

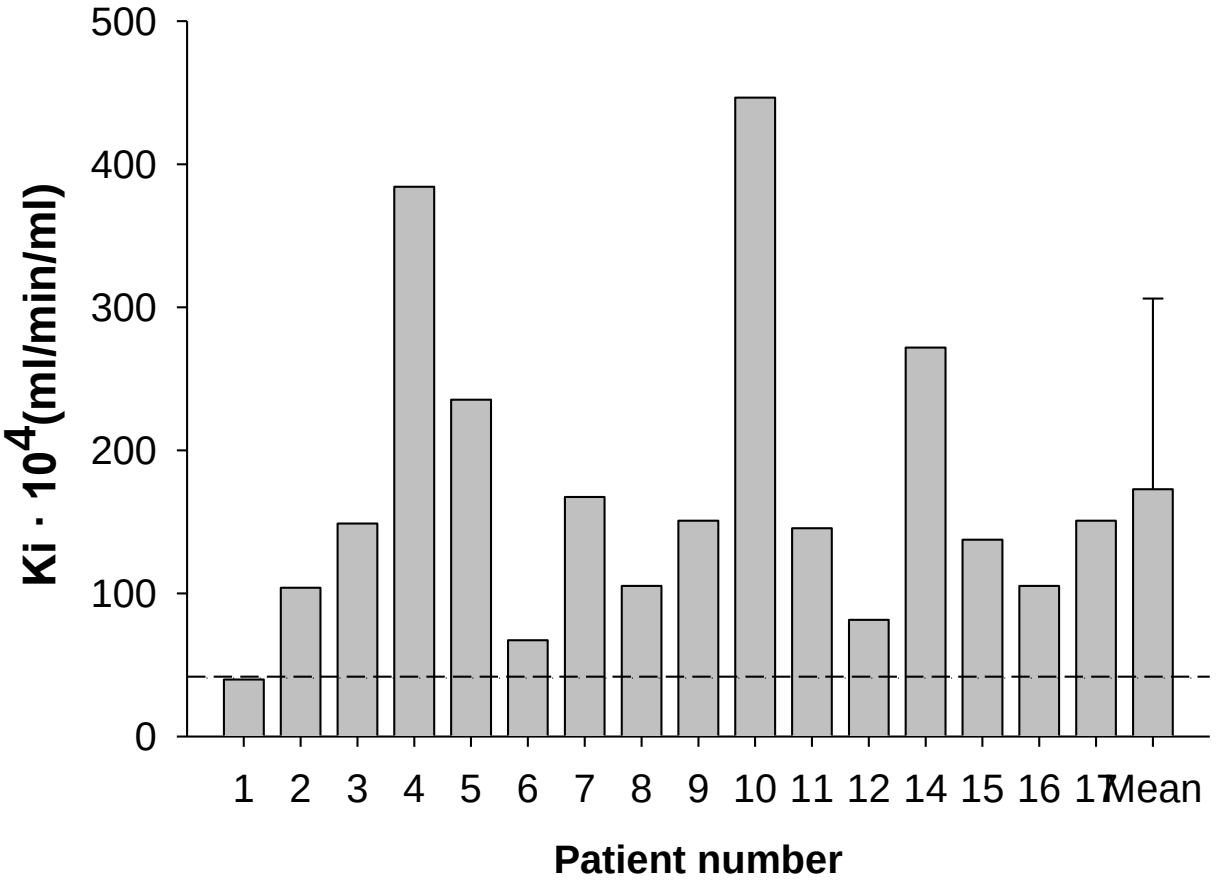
500
400
300
200
100
0
Ki · 10^4(ml/min/ml)
1
2
3
4
5
6
7
8
9
10
11
12
14
15
16
17
Mean
Patient number

FIGURE 3A

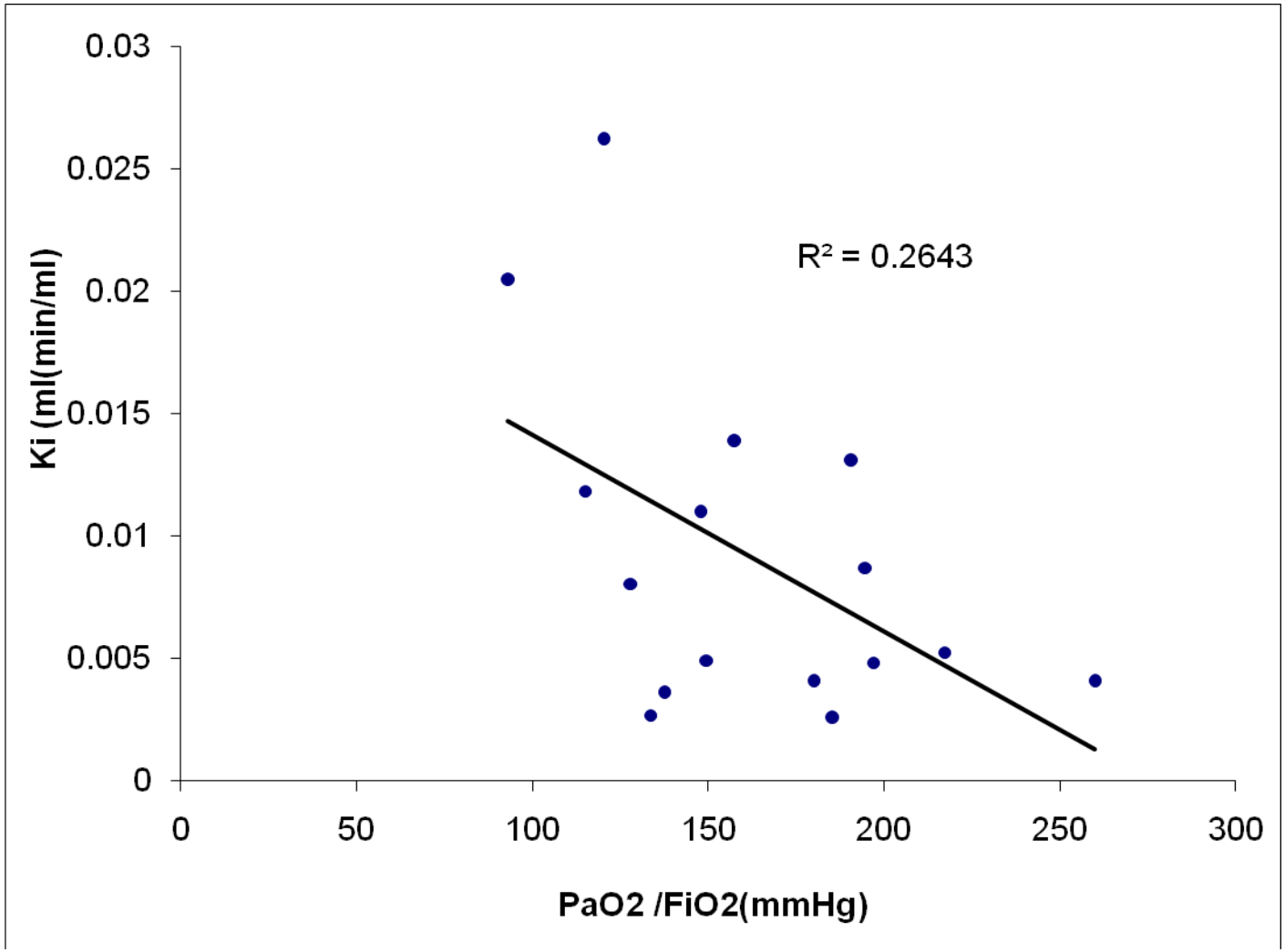
0.03
0.025
0.02
0.015
0.01
0.005
0
Ki (ml(min/ml)
R² = 0.2643
0
50
100
150
200
250
300
PaO2 /FiO2(mmHg)

FIGURE 3B

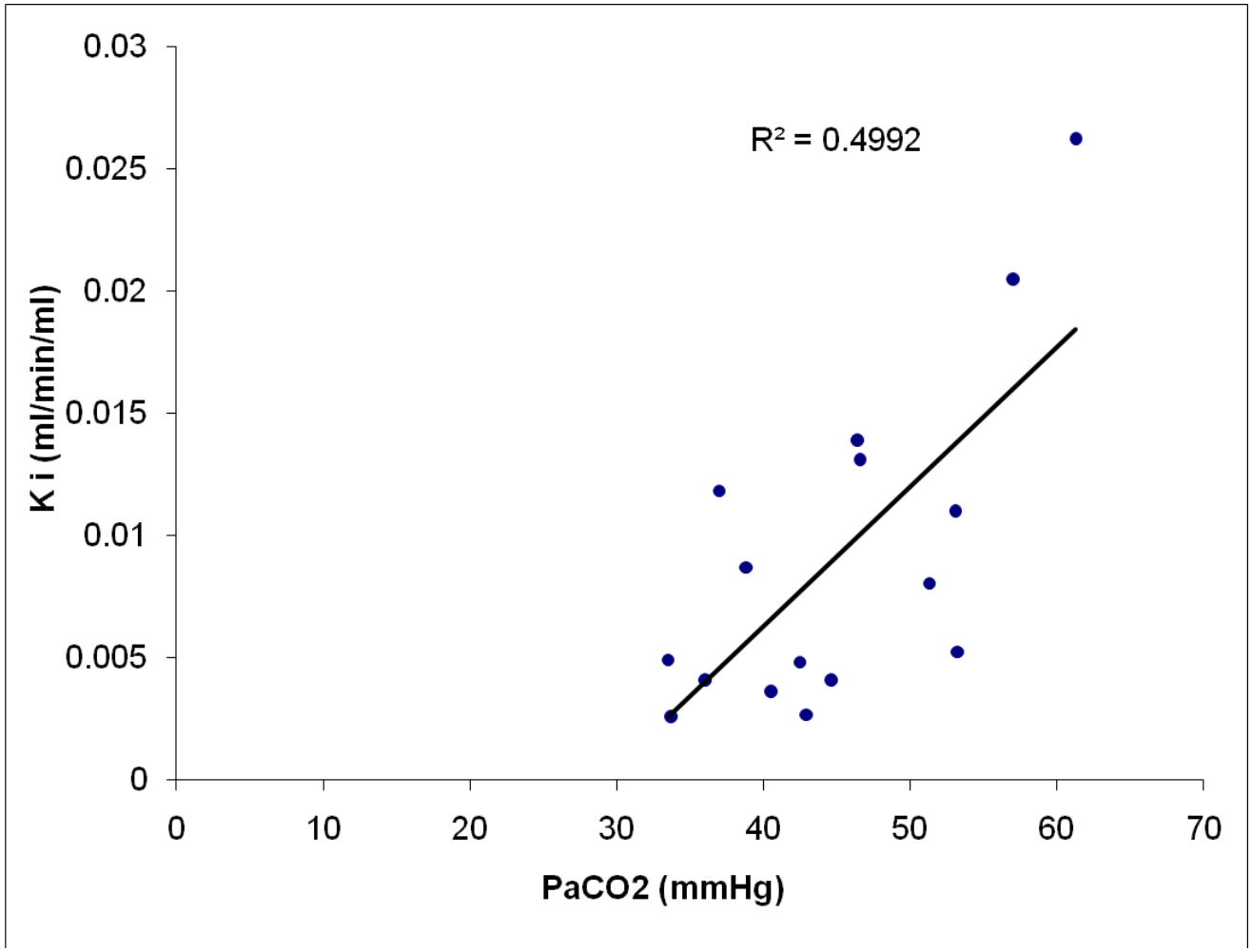
0.03
0.025
0.02
0.015
0.01
0.005
0
K i (ml/min/ml)
R² = 0.4992
0
10
20
30
40
50
60
70
PaCO2 (mmHg)

FIGURE 4

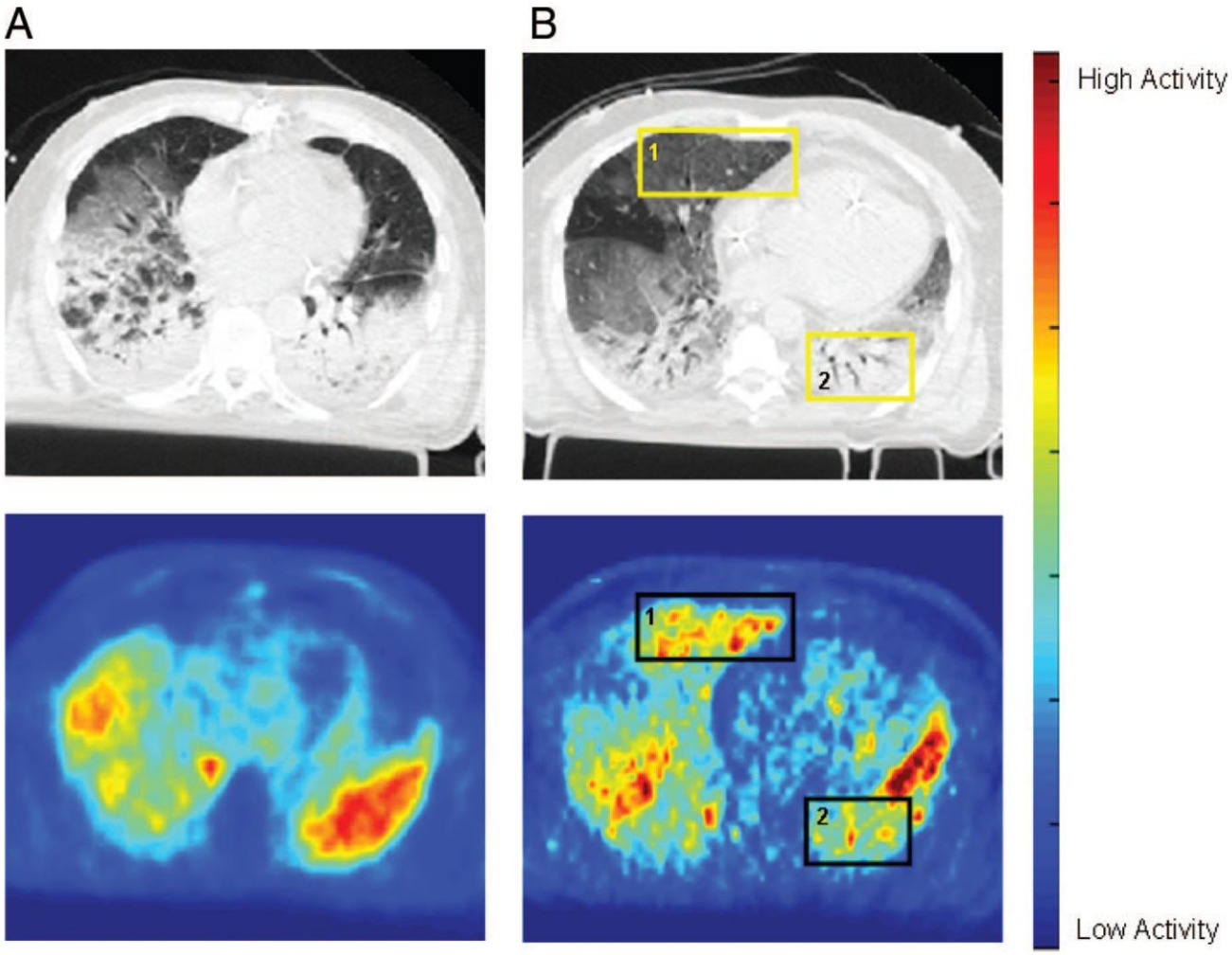

FIGURE 5

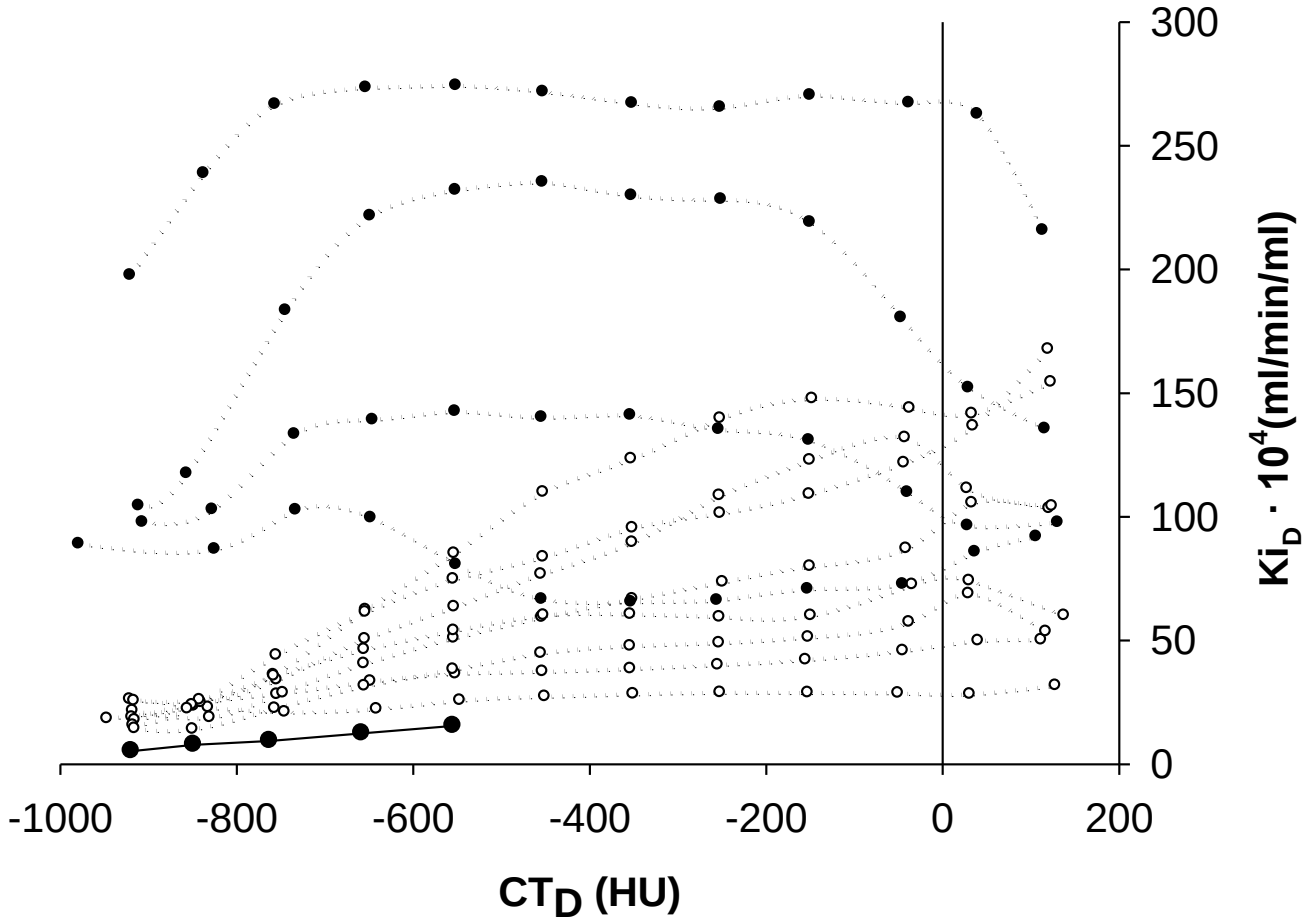
300
250
200
150
100
50
0
$Ki_D \cdot 10^4$(ml/min/ml)
-1000
-800
-600
-400
-200
0
200
CT_D (HU)

FIGURE 7

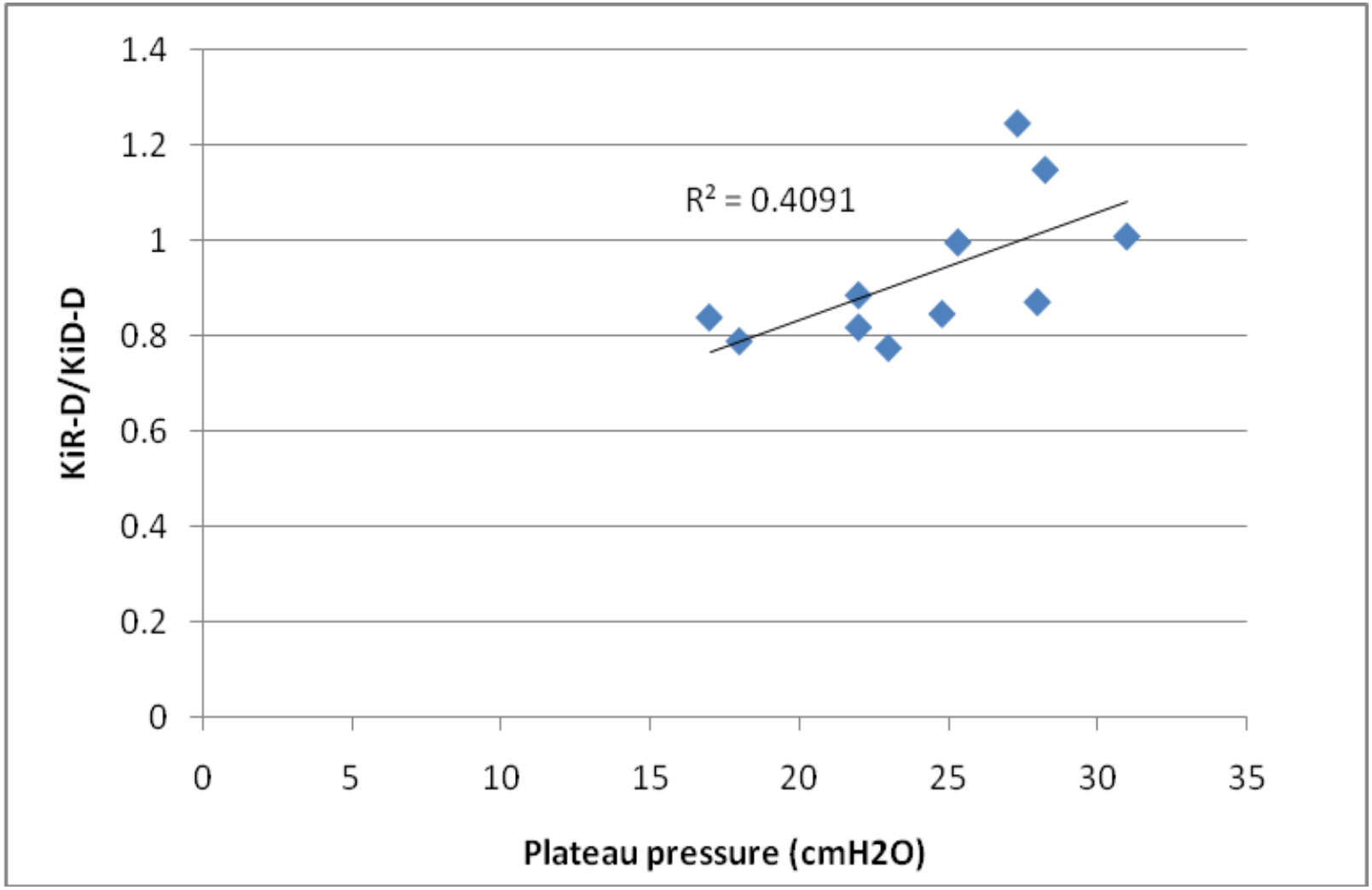
1.4
1.2
1
0.8
0.6
0.4
0.2
0
KiR-D/KiD-D
R² = 0.4091
0
5
10
15
20
25
30
35
Plateau pressure (cmH2O)

FIGURE 8A

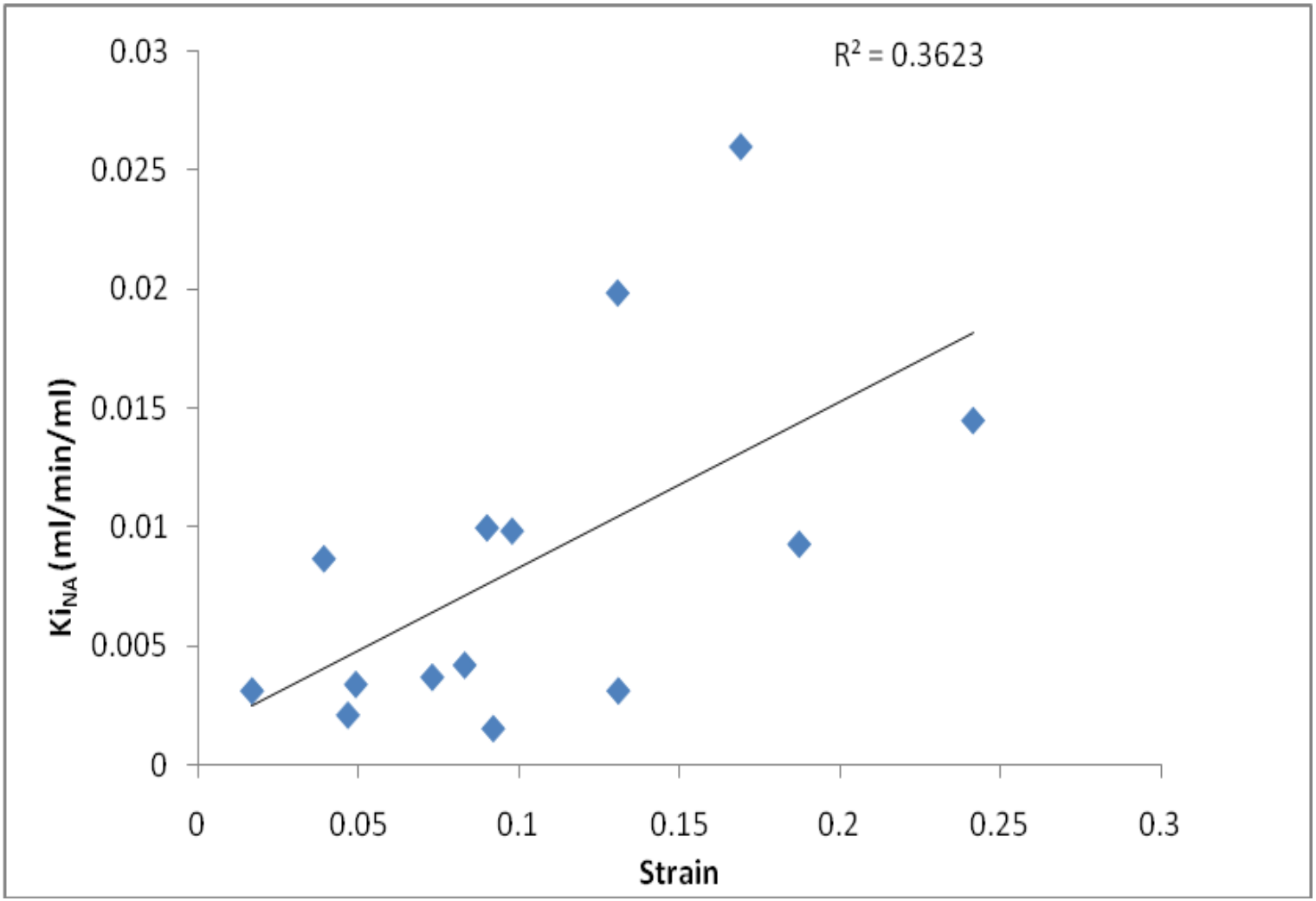
R² = 0.3623
0.03
0.025
0.02
0.015
0.01
0.005
0
Ki_NA (ml/min/ml)
0
0.05
0.1
0.15
0.2
0.25
0.3
Strain

FIGURE 8B

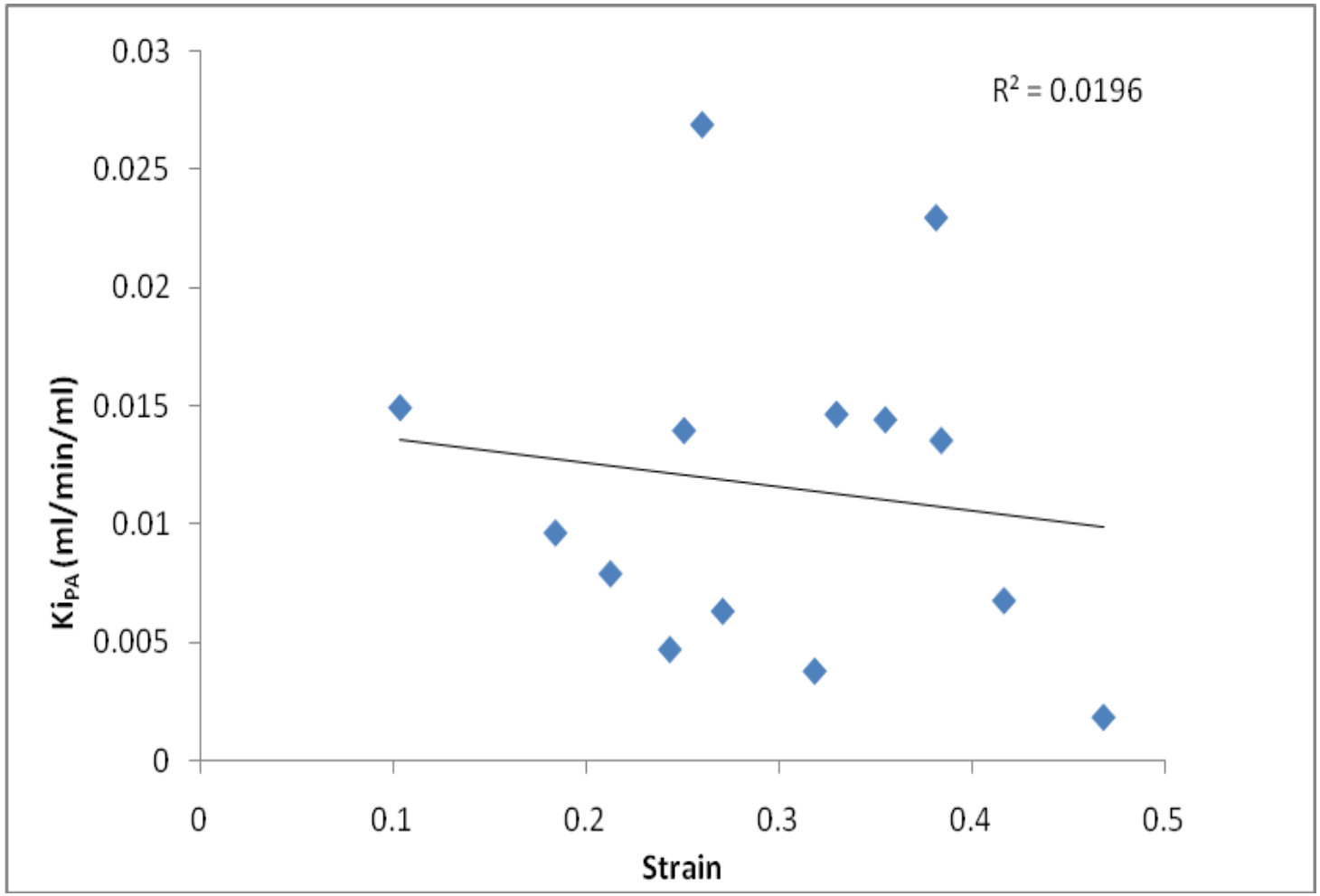
0.03
0.025
0.02
0.015
0.01
0.005
0
Ki_{PA} (ml/min/ml)
R^2 = 0.0196
0
0.1
0.2
0.3
0.4
0.5
Strain

FIGURE 9A

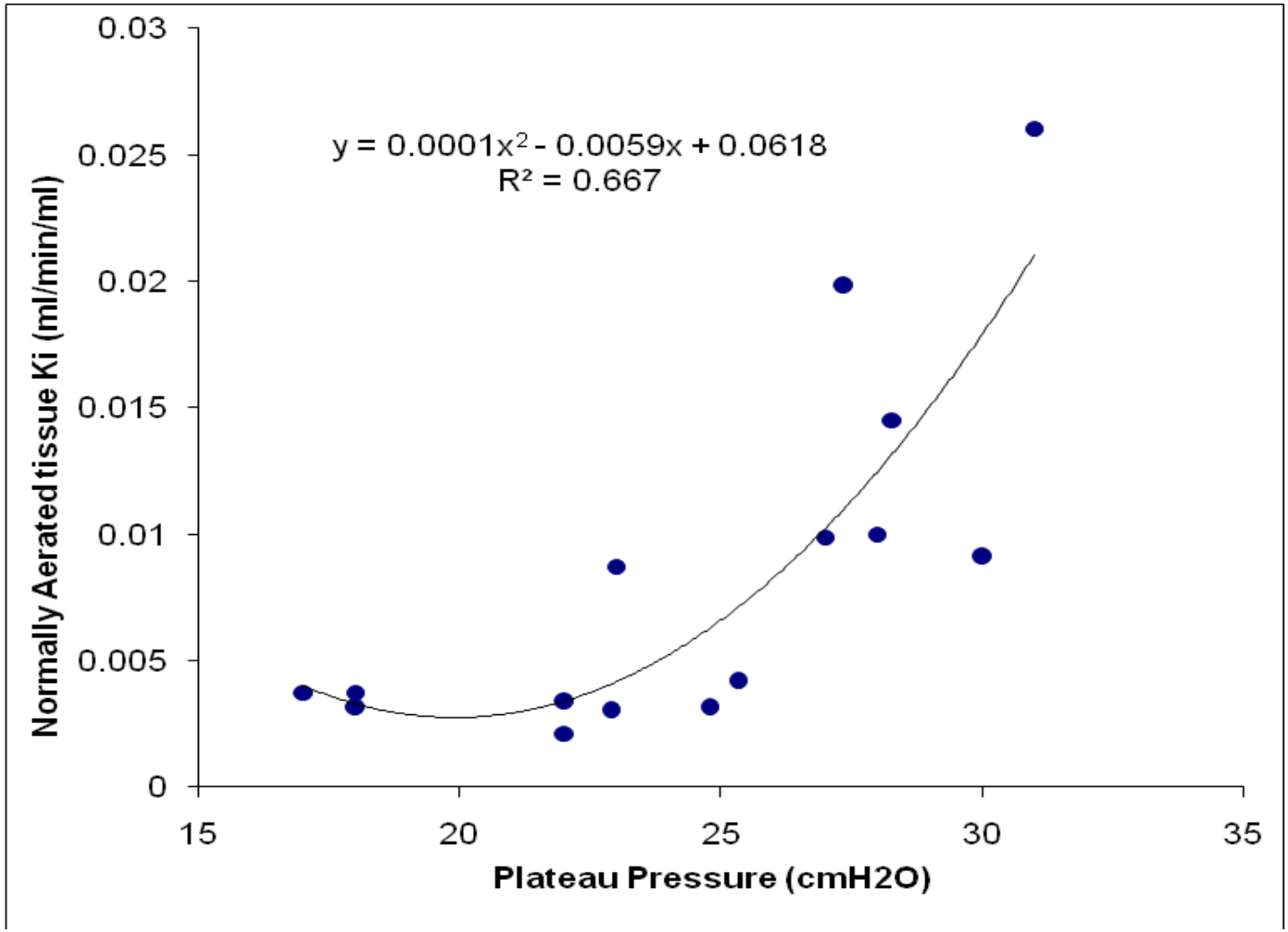
y = 0.0001x² - 0.0059x + 0.0618
R² = 0.667
Normally Aerated tissue Ki (ml/min/ml)
0.03
0.025
0.02
0.015
0.01
0.005
0
15
20
25
30
35
Plateau Pressure (cmH2O)

FIGURE 9B

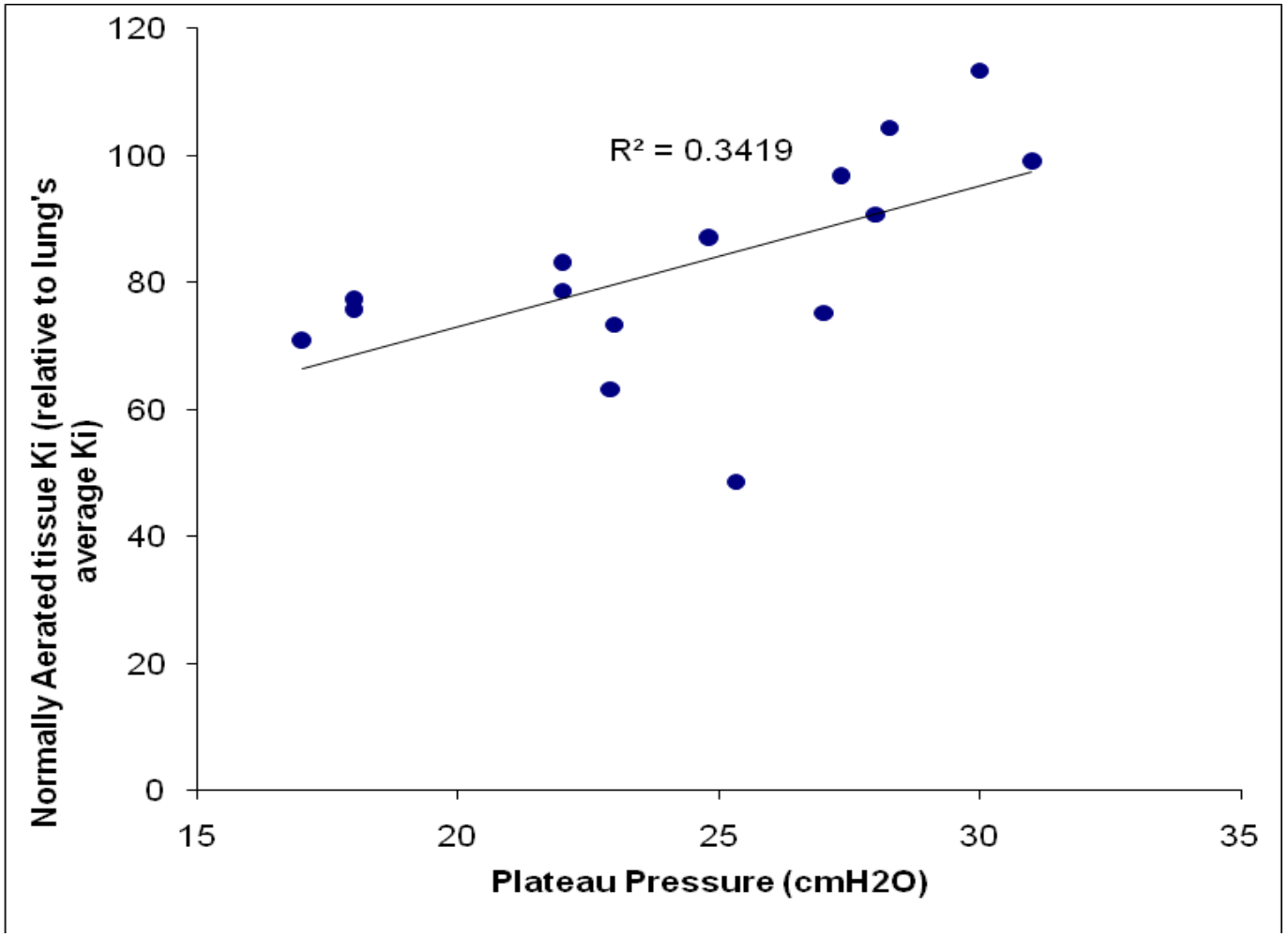
120
100
80
60
40
20
0
15
20
25
30
35
R² = 0.3419
Normally Aerated tissue Ki (relative to lung's average Ki)
Plateau Pressure (cmH2O)